R. & M. No. 3406

MINISTRY OF AVIATION

AERONAUTICAL RESEARCH COUNCIL
REPORTS AND MEMORANDA

Design of Warped Slender Wings with the Attachment Line along the Leading Edge

By J. Weber

LONDON: HER MAJESTY'S STATIONERY OFFICE
1965
PRICE 15*s.* 6*d.* NET

Design of Warped Slender Wings with the Attachment Line along the Leading Edge

By J. Weber

Communicated by the Director-General of Scientific Research (Air), Ministry of Supply

*Reports and Memoranda No. 3406**

September, 1957

Summary.

This report deals with the design of slender warped wings with unswept trailing edge but otherwise arbitrary planform which have, at the design lift coefficient, zero load along the leading edge and a near planar vortex sheet from the trailing edge. The wing can have an arbitrary chordwise curvature on which a spanwise curvature is superposed so that in any spanwise section the wing is straight over the inner part of the wing and curved over the portion near to the leading edges; the position of this change can vary arbitrarily in the chordwise direction. Formulae and working charts are given for determining the local load coefficient (and with it the streamwise velocity component), the spanwise velocity component, the total lift coefficient and the total drag. Numerical examples, for the gothic planform, are given to illustrate some of the effects of the various parameters on the load distribution, the section shapes and the drag. Slender-wing theory has been applied except for determining the wave drag which has been obtained from an approximate relation derived by the not-so-slender theory of Adams and Sears.

LIST OF CONTENTS

* Replaces R.A.E. Tech. Note No. Aero. 2530—A.R.C. 20 051.

LIST OF CONTENTS—*continued*

LIST OF APPENDICES

LIST OF ILLUSTRATIONS

---

1. *Introduction.*

The flow past a wing with a highly swept leading edge at incidence usually separates at the edge forming a vortex layer, which rolls up into a rotating core lying above and inboard of the edge. Sharp edges are thought to be desirable on slender wings so that the conditions under which this separation occurs are determined. With these slender, sharp-edged wings separation will occur from all edges except in special cases, of which the flat plate at zero incidence is an example. As the incidence of a wing increases from negative to positive values, the attachment line near the leading edge (*see* Maskell[1]) moves from being entirely on the upper surface to being entirely on the lower surface and vortex cores form below and above the wing respectively. However, unless the warp of the wing (the term 'warp' is used in the following to describe camber and twist together) is specially designed, there will be a range of incidence for which the attachment line crosses the leading edge and this point of intersection will vary with the incidence. This undesirable phenomenon is avoided on a wing for which the attachment line lies all along the leading edge at some incidence. No separation takes place at this incidence, at higher or lower values the vortex cores lie entirely above or below the surface.

The simplest form of warp satisfying this condition is the flat plate. On a flat plate the flow separates at any non-zero lift from all edges. Under these conditions the vortex drag of a delta wing substantially exceeds the value for a wing with trailing-edge separation only, at least in the range of lift coefficient where the maximum lift-drag ratio is expected to be found[2 to 4]. The use of other planforms may modify this result to some extent[5]; but, certainly for wings not too far removed from the delta, it is desirable to design cambered surfaces to have separation only from the trailing edge at some non-zero lift coefficient. The condition for this is that the attachment line should lie along the leading edge for its whole length. According to attached-flow theory, the local load at a subsonic leading edge of a thin wing with finite slope to the free-stream direction is either infinite or zero. The latter case occurs when the attachment line is along the leading edge. In accordance with the account of separation given above, it is only in this case that attached-flow theory can be expected to apply to a slender wing, and it is only in this case that we use it. Thus no attempt is made to realise a flow with theoretically infinite suction peaks at the leading edge. On the contrary, warped surfaces are proposed which in their design condition have vanishing load at the leading edge, combined with suction forces on forward-facing surfaces inboard of it. These wings have in this way values of the vortex drag which are almost as low as those predicted by the unrealisable attached flow past the flat wing at incidence.

Many different warped wings can be designed on which theory predicts the attachment line to lie along the leading edge and the vortex drag to be low. Whether these properties persist in a real flow depends on the development of the region where viscous forces are dominant and thus on the pressure distribution over the wing. The pressure gradients occurring along streamlines in the flow over the wing with finite thickness will to some extent decide whether flow separations and shock waves inboard of the leading edge are avoided. Furthermore, the value of the load which can be maintained at the trailing edge when the main stream is supersonic is limited by the shock system there, which cannot be studied by the present theory.

The choice of a wing shape will further depend on the pressure distribution at off-design conditions. The aim is to achieve with increasing lift coefficient a smooth variation of the flow field which is dominated by the primary separation developing from the leading edge and not by a secondary separation somewhere inboard on the wing.

The planform and camber surface, to be chosen for a practical design, are also affected by considerations outside the field of aerodynamics. For example, it may be desirable to have a curved centre section of the wing so that, at the design lift coefficient, the incidence at which the centre section is set against the main stream is smaller than for the uncambered centre section, with the same slope at the trailing edge. This brings a reduction of the difference in height between the nose and the trailing edge of the wing and thus, presumably, in the height of the undercarriage. These remarks show that we require a family of wing shapes with several free parameters from which to choose.

In this report, thin slender wings of arbitrary planform but with unswept trailing edges are treated. The chordwise curvature of the centre section of the wing is arbitrary, but only some special types of spanwise curvature are considered. In a spanwise section the wing is straight over the inner part and curved over the portion near to the leading edges. The spanwise position of this 'shoulder', where the spanwise curvature begins, is a free parameter which can vary along the chord. Two different types of curvature are considered; the surface slope outboard of the shoulder varies either linearly or quadratically across the span, as in the case of wings with conical flow treated by Brebner[6]. For completeness, the case of constant surface slope over the outer part is also included, though the corresponding load distribution has logarithmically infinite values at the shoulder as a consequence of the discontinuous change of the wing slope.

In this report, formulae are given for the local load distribution (and thus within linear theory for the streamwise velocity increment) and for the spanwise velocity component. The total lift and the vortex drag are determined, and the chordwise distribution of the cross load, required for calculating the wave drag, is also determined. The given formulae apply to any slender smooth planform with unswept trailing edges. Numerical examples have been worked out for the so-called 'gothic' planform which has a pointed nose, streamwise tips and parabolically varying leading edges. The pitching moments have not been determined.

2. *General Outline of the Method.*

The theory of lifting wings of given planform usually deals with one of the following three problems:

(i) The load distribution is given and the shape of the wing, which has the required load distribution, is to be determined.

(ii) The wing shape is given and the load distribution which this wing has in a given flow is to be determined.

(iii) The wing shape is to be found which produces the minimum drag due to lift for a given amount of total lift.

When solving our special problem by the first method, it is of course easy to satisfy the requirement of zero load at the leading edge. It is more difficult to prescribe load distributions which satisfy the requirement of lowish drag. The properties of the pressure distribution would of course depend on the prescribed load distribution. If we express the latter as a finite series of some basic solutions (as e.g. in Ref. 7), then the pressure distributions as well as the resulting wing shapes may exhibit some waviness. A chordwise waviness in the pressure distribution implies the undesirable feature of having several compressions on the wing.

The second method is unsuitable for solving our problem, since, for arbitrary planforms, it is impossible to guess a wing shape such that at some $\overline{C}_L$ the attachment line shall lie along the whole leading edge. Only if the distribution of surface slope is conical can it be assumed *a priori* that the attachment line will occur at the leading edge for some $\overline{C}_L$.

The methods developed for solving the third problem of wing theory are not applicable to our task, since the leading-edge condition does not fit in. We want to design wings of general planform and there are cases, as e.g. the delta planform, for which the condition of minimum vortex drag is incompatible with the condition of zero load at the leading edge. The latter leads to a spanwise distribution of the chord load which has zero slope at the tips, whilst the condition of minimum vortex drag requires an elliptic distribution. We do not restrict our design problem to the cases where the total lift-dependent drag is exactly at R. T. Jones' lower bound[8, 9], but require that it should be reasonably low.

It has been found convenient for solving our problem to apply a mixed procedure by prescribing the wing shape to some extent only and prescribing some properties of the load distribution. Apart from the consideration of more general planforms, it is mainly in this respect that the present treatment differs from that of Smith and Mangler[7]. The present method has been applied by Brebner[6] to conical flow. We prescribe a certain type of downwash distribution over the wing (i.e. within linear theory, of the chordwise wing slope $\partial z/\partial x$), but leave the ratio between the downwash at the leading edge and that at the centre of the wing free so that we can satisfy the condition of zero load at the leading edge. In some cases, we introduce the further condition that the spanwise distribution of the chord load at the trailing edge is elliptic to obtain minimum vortex drag. We do not introduce a condition concerning the wave drag but shall find that among the large number of solutions there are some for which the drag value is close to the lower bound of R. T. Jones.

The calculations are based on slender-wing theory except for the wave drag which is determined by applying the not-so-slender thin-wing theory of Adams and Sears[9].

We begin with a required type of spanwise downwash distribution, which contains a free parameter to be determined later. A solution of the two-dimensional Laplace equation for the velocity potential is taken which produces the required downwash distribution. The velocity potential gives the spanwise distribution of the local chord load, from which the local load is obtained by differentiation in the chordwise direction. The free parameter in the downwash distribution can then be chosen such that the local load at the leading edge is zero. The spanwise velocity component is obtained from the spanwise distribution of the local chord load by differentiation in the spanwise direction. The spanwise distribution of the chord load at the trailing edge determines the total lift

and the vortex drag. For determining the wave drag the chordwise distribution of the cross load is required. This is obtained by integrating the local load coefficient across the span.

The above procedure is not only simple but has further advantages. It guarantees that the resulting shapes do not exhibit any waviness and allows certain properties of the shape to be prescribed as e.g. the spanwise extent of the inner part of the wing which is uncambered in spanwise sections. The leading-edge condition is automatically fulfilled and the condition of minimum vortex drag can be fed in. The method can be applied to slender wings with unswept trailing edge but arbitrary shape of the centre section and the leading edge. A number of results can be written in closed form.

3. *Details of the Method.*

3.1. *Geometry of the Wings Considered.*

A right-handed system of Cartesian co-ordinates x, y, z is used. The origin is at the leading edge of the centre section, the x-axis in the direction of the undisturbed stream, y spanwise and z positive upwards. The wing chord c_0 at the centre section of the wing is taken as unity throughout.

The planform of the wing is given by

$$|y| \leqslant s(x). \tag{1}$$

$s(x)$ and its first derivative with respect to x, $ds(x)/dx$, are assumed to be continuous for $0 \leqslant x \leqslant 1$. The wings considered have curved or straight sweptback leading edges such that the forward part of the wing is pointed, i.e. $s(0) = 0$, $s'\{ds(x)/dx\}_{x=0}$ is finite. In a planview the trailing edges of the wings are unswept. The planforms are such that the maximum span is reached at the trailing edge. The value of the semispan at the trailing edge is denoted by

$$s(1) = s_T. \tag{2}$$

We consider slender wings only, so that $s_T/c_0 \ll 1$. The theory is developed for arbitrary functions $s(x)$, but the numerical examples given in this report are calculated for the so-called gothic planform:

$$s(x) = s_T x(2-x). \tag{3}$$

The shape $z(x, y)$ of the wing surface is determined as that of a stream surface in the known velocity field by applying the linearized boundary condition.

$$\frac{\partial z(x, y)}{\partial x} = \frac{v_z(x, y, 0)}{V_0} \tag{4}$$

where V_0 is the velocity of the undisturbed stream and $v_z(x, y, 0)$ the velocity component normal to the chordal plane of the wing.

As mentioned before, we begin by prescribing the spanwise distribution of v_z. Three different distributions of the downwash will be treated in this report (*see* Fig. 1). Using the notation

$$\eta = \frac{y}{s(x)}, \tag{5}$$

they are:

$$-\frac{v_z(x, y, 0)}{V_0} = \begin{cases} C(x) & \text{for } 0 \leqslant |\eta| \leqslant \eta_0(x) \\ C(x) + D_\nu(x)\left[\dfrac{|\eta| - \eta_0(x)}{1 - \eta_0(x)}\right]^{\nu-1} & \text{for } \eta_0(x) \leqslant |\eta| \leqslant 1 \end{cases} \tag{6}$$

where $\nu = 1, 2, 3$.

The distributions considered are thus such that for spanwise sections, $x = \text{const.}$, the slope $\partial z(y; x)/\partial x$ is constant over the inner part of the wing $0 < |\eta| < \eta_0(x)$. Over the outer part of the

wing, $|\eta| > \eta_0(x)$, $\partial z/\partial x$ is given by a different expression. It is either constant or varies linearly or quadratically. The shape of the inner part of the wing is determined by the choice of $C(x)$. The centre section in particular can be straight or curved, depending on $C(x)$. The values of $C(x)$ and $\eta_0(x)$ can be chosen arbitrarily but the values of $D_\nu(x)$ depend on $C(x)$ and $\eta_0(x)$ in such a way that the condition of zero load at the leading edge is satisfied. The relations between $D_\nu(x)$, $C(x)$ and $\eta_0(x)$ will be derived in Section 3.3.

Anticipating the results of Section 3.3, we may rewrite the three types of downwash distribution in the form

$$\text{(i)} \quad -\frac{v_z(x, y, 0)}{V_0} = \begin{cases} C(x) & \text{for } 0 < |\eta| < \eta_0(x) \\ -C(x)\left(\dfrac{\pi/2}{\cos^{-1}\eta_0} - 1\right) & \text{for } \eta_0(x) < |\eta| < 1 \end{cases} \tag{7}$$

$$\text{(ii)} \quad -\frac{v_z(x, y, 0)}{V_0} = \begin{cases} C(x) & \text{for } 0 < |\eta| < \eta_0(x) \\ C(x)\left[1 - \dfrac{\pi(|\eta| - \eta_0)}{2\{\sqrt{(1-\eta_0^2)} - \eta_0 \cos^{-1}\eta_0\}}\right] & \text{for } \eta_0(x) < |\eta| < 1 \end{cases} \tag{8}$$

$$\text{(iii)} \quad -\frac{v_z(x, y, 0)}{V_0} = \begin{cases} C(x) & \text{for } 0 < |\eta| < \eta_0(x) \\ C(x)\left[1 - \dfrac{\pi(|\eta| - \eta_0)^2}{(1+2\eta_0^2)\cos^{-1}\eta_0 - 3\eta_0\sqrt{(1-\eta_0^2)}}\right] & \text{for } \eta_0(x) < |\eta| < 1\,. \end{cases} \tag{9}$$

The ratio between the downwash required at the leading edge and the value at the inner part of the wing, to achieve zero load at the leading edge, is:

$$\frac{v_z(\eta = 1)}{v_z(\eta = 0)} = 1 + \frac{D_\nu(x)}{C(x)}; \tag{10}$$

it is plotted in Fig. 2. The figure shows that the slope at the leading edge is larger the closer the shoulder η_0 is to the leading edge and that for quadratically varying downwash the required slope at the leading edge is larger than for the linearly varying one, if we compare for the same η_0.

From the known slope $\partial z(x, y)/\partial x$ of the wing surface the shape of chordwise sections $z(x, y = \text{const.})$ can be determined by integration except for an additive term $f(y)$. The choice of the function $f(y)$, which in linear theory is arbitrary, determines the spanwise shape of the trailing edge. In our numerical examples, we have chosen such a value of $f(y)$ that the trailing edge becomes a straight line, $z(1, y) = z(1, 0) = z_T$,

$$z(x, y) = z(1, y) - \int_x^1 \frac{\partial z(x', y)}{\partial x'}\, dx'. \tag{11}$$

This implies that the leading edge is not planar.

3.2. *Spanwise Distribution of the Local Chord Load for Various Downwash Distributions.*

As a starting point, we will derive in this section a relation between the spanwise distribution of the local chord load $L(x, y)$ and the local downwash $-v_z(x, y)$. The local chord load $L(x, y)$ is the integral at a station $y = \text{const.}$ of the local load coefficient $l(x, y)$ from the leading edge to the station x considered:

$$L(x, y) = \int_{x_{\mathrm{LE}}(y)}^{x} l(x', y)dx' \tag{12}$$

The local load coefficient $l(x, y)$ is defined by

$$\begin{aligned} l(x, y) &= -\Delta C_p(x, y) \\ &= -[C_{p\mathrm{U}}(x, y) - C_{p\mathrm{L}}(x, y)] \end{aligned} \tag{13}$$

where the suffices U and L denote the upper and lower surfaces of the wing. In slender-wing theory Bernoulli's equation is applied in the form

$$C_p = \frac{p - p_0}{\frac{1}{2}\rho_0 V_0^2} = -2\frac{v_x}{V_0} - \frac{v_y^2 + v_z^2}{V_0^2}. \tag{14}$$

With wings on which the flow separates only from the trailing edge, we can, to a first order, approximate wing and wake by a planar distribution of singularities, even though the camber may be appreciable. For planar sheets the term v_y^2 is the same on the upper and lower surfaces, if we ignore the contribution of the sources which would represent the finite thickness of the wing. In this case

$$\begin{aligned} l(x, y) &= 2\left[\frac{v_{x\mathrm{U}}(x, y)}{V_0} - \frac{v_{x\mathrm{L}}(x, y)}{V_0}\right] \\ &= \frac{2}{V_0}\left[\frac{\partial\phi_{\mathrm{U}}(x, y)}{\partial x} - \frac{\partial\phi_{\mathrm{L}}(x, y)}{\partial x}\right] \end{aligned} \tag{15}$$

where ϕ is the perturbation velocity potential in the plane $x = 0$.

Using equations (12) and (15), we find that $L(x, y)$ is related to the difference in the potential function on the upper and lower surfaces of the wing, $\Delta\phi(x, y) = \phi_{\mathrm{U}}(x, y) - \phi_{\mathrm{L}}(x, y)$, by:

$$L(x, y) = \frac{2}{V_0}\Delta\phi(x, y). \tag{16}$$

$\Delta\phi(x, y)$ is equal to the circulation $\Gamma(x, y)$ around the part of the wing in front of the station $x = \text{const.}$ and outboard of $y = \text{const.}$

In slender-wing theory the velocity potential $\phi(x, y)$ is a solution of the two-dimensional Laplace equation:

$$\frac{\partial^2\phi}{\partial y^2} + \frac{\partial^2\phi}{\partial z^2} = 0. \tag{17}$$

We have to find the solution which gives for each station $x = \text{const.}$ in the plane $z = 0$ the required normal velocity component $v_z(y, z = 0; x)$. To solve this problem is equivalent to determining the strength $d\Gamma(y; x)/dy$ of a system of two-dimensional vortices (in the plane $z = 0$ and parallel to the x-axis) which produce the given velocity $v_z(y; x)$:

$$v_z(y; x) = -\frac{1}{2\pi}\int_{-s(x)}^{s(x)} \frac{d\Gamma(y'; x)}{dy'}\frac{dy'}{y - y'}. \tag{18}$$

The solution of this integral equation reads (*see* e.g. Ref. 10):

$$\frac{\Gamma(y; x)}{2s(x)V_0} = \frac{1}{\pi}\int_0^{\pi} \frac{v_z(\vartheta'; x)}{V_0}\sin\vartheta' \log\frac{\sin\frac{|\vartheta - \vartheta'|}{2}}{\sin\frac{\vartheta + \vartheta'}{2}}\,d\vartheta' \tag{19}$$

where $\cos\vartheta = \eta = y/s(x)$.

Equation (19) enables Γ to be found for the velocity distributions

$$-\frac{v_z(y; x)}{V_0} = \begin{cases} 0 & \text{for } 0 < |\eta| < \eta_0 \\ D_\nu(x)\left[\dfrac{|\eta| - \eta_0(x)}{1 - \eta_0(x)}\right]^{\nu-1} & \text{for } \eta_0 < |\eta| < 1. \end{cases}$$

The cases $\nu = 1$ and 2 were calculated by Watson[10].

Superposing the elliptic spanwise distribution of the chord load, corresponding to a constant $-v_z(y;x) = C(x)$ for $0 < |\eta| < 1$, we obtain for the velocity distributions of equation (6) the spanwise distributions of the chord load:

$$L_1(x,y) = 4C(x)s(x)\sqrt{(1-\eta^2)} + \frac{4}{\pi} D_1(x)s(x) \left\{ 2\cos^{-1}\eta_0 \sqrt{(1-\eta^2)} + \right.$$
$$\left. + \eta_0 \ln \frac{|\sqrt{(1-\eta^2)} - \sqrt{(1-\eta_0^2)}|}{\sqrt{(1-\eta^2)} + \sqrt{(1-\eta_0^2)}} - \eta \ln \frac{|\eta_0\sqrt{(1-\eta^2)} - \eta\sqrt{(1-\eta_0^2)}|}{\eta_0\sqrt{(1-\eta^2)} + \eta\sqrt{(1-\eta_0^2)}} \right\} \tag{20}$$

$$L_2(x,y) = 4C(x)s(x)\sqrt{(1-\eta^2)} + \frac{4}{\pi(1-\eta_0)} D_2(x)s(x) \left[\{\sqrt{(1-\eta_0^2)} - 2\eta_0 \cos^{-1}\eta_0\}\sqrt{(1-\eta^2)} - \right.$$
$$\left. - \frac{\eta_0^2 + \eta^2}{2} \ln \frac{|\sqrt{(1-\eta^2)} - \sqrt{(1-\eta_0^2)}|}{\sqrt{(1-\eta^2)} + \sqrt{(1-\eta_0^2)}} + \eta_0\eta \ln \frac{|\eta_0\sqrt{(1-\eta^2)} - \eta\sqrt{(1-\eta_0^2)}|}{\eta_0\sqrt{(1-\eta^2)} + \eta\sqrt{(1-\eta_0^2)}} \right] \tag{21}$$

$$L_3(x,y) = 4C(x)s(x)\sqrt{(1-\eta^2)} + \frac{4}{3\pi(1-\eta_0)^2} D_3(x)s(x) \times$$
$$\times \left[\{(1+2\eta^2+6\eta_0^2)\cos^{-1}\eta_0 - 5\eta_0\sqrt{(1-\eta_0^2)}\}\sqrt{(1-\eta^2)} + \right.$$
$$+ (\eta_0^3+3\eta_0\eta^2) \ln \frac{|\sqrt{(1-\eta^2)} - \sqrt{(1-\eta_0^2)}|}{\sqrt{(1-\eta^2)} + \sqrt{(1-\eta_0^2)}} -$$
$$\left. - (\eta^3+3\eta_0^2\eta) \ln \frac{|\eta_0\sqrt{(1-\eta^2)} - \eta\sqrt{(1-\eta_0^2)}|}{\eta_0\sqrt{(1-\eta^2)} + \eta\sqrt{(1-\eta_0^2)}} \right]. \tag{22}$$

Anticipating again the relations (28) to (30) between $D_\nu(x)$ and $C(x)$ and $\eta_0(x)$ from Section 3.3, we obtain for the spanwise distributions of the chord load:

$$L_1(x,y) = C(x)s(x) \frac{2}{\cos^{-1}\eta_0} \left\{ - \eta_0 \ln \frac{|\sqrt{(1-\eta^2)} - \sqrt{(1-\eta_0^2)}|}{\sqrt{(1-\eta^2)} + \sqrt{(1-\eta_0^2)}} + \right.$$
$$\left. + \eta \ln \frac{|\eta_0\sqrt{(1-\eta^2)} - \eta\sqrt{(1-\eta_0^2)}|}{\eta_0\sqrt{(1-\eta^2)} + \eta\sqrt{(1-\eta_0^2)}} \right\}. \tag{23}$$

$$L_2(x,y) = C(x)s(x) \frac{1}{\sqrt{(1-\eta_0^2)} - \eta_0 \cos^{-1}\eta_0} \left\{ 2\sqrt{(1-\eta_0^2)}\sqrt{(1-\eta^2)} + \right.$$
$$+ (\eta_0^2+\eta^2) \ln \frac{|\sqrt{(1-\eta^2)} - \sqrt{(1-\eta_0^2)}|}{\sqrt{(1-\eta^2)} + \sqrt{(1-\eta_0^2)}} -$$
$$\left. - 2\eta_0\eta \ln \frac{|\eta_0\sqrt{(1-\eta^2)} - \eta\sqrt{(1-\eta_0^2)}|}{\eta_0\sqrt{(1-\eta^2)} + \eta\sqrt{(1-\eta_0^2)}} \right\}. \tag{24}$$

$$L_3(x,y) = C(x)s(x) \frac{4}{3[(1+2\eta_0^2)\cos^{-1}\eta_0 - 3\eta_0\sqrt{(1-\eta_0^2)}]} \times$$
$$\times \left[\{2(1-\eta^2)\cos^{-1}\eta_0 - 4\eta_0\sqrt{(1-\eta_0^2)}\}\sqrt{(1-\eta^2)} - \right.$$
$$- (\eta_0^3+3\eta_0\eta^2) \ln \frac{|\sqrt{(1-\eta^2)} - \sqrt{(1-\eta_0^2)}|}{\sqrt{(1-\eta^2)} + \sqrt{(1-\eta_0^2)}} +$$
$$\left. + (\eta^3+3\eta_0^2\eta) \ln \frac{|\eta_0\sqrt{(1-\eta^2)} - \eta\sqrt{(1-\eta_0^2)}|}{\eta_0\sqrt{(1-\eta^2)} + \eta\sqrt{(1-\eta_0^2)}} \right]. \tag{25}$$

The limit of $L_\nu(x, y)$ as η_0 tends to 1 is, of course, for all three cases the elliptic loading function:

$$L(x, y) = C(x)s(x)4\sqrt{(1-\eta^2)}. \tag{26}$$

3.3. *Local Load Distributions.*

Knowing the local chord load, we can now determine the local load $l_\nu(x, y)$ by differentiation·

$$l_\nu(x, y) = \frac{\partial L_\nu(x, y)}{\partial x}. \tag{27}$$

In particular, we can determine by equations (20) to (22) the load at the leading edge, $l(x, \eta = 1)$. The condition of zero load at the leading edge leads to the following relations between $D_\nu(x)$ and $C(x)$ and $\eta_0(x)$:

$$D_1(x) = -\frac{\pi/2}{\cos^{-1}\eta_0(x)} C(x) \tag{28}$$

$$D_2(x) = -\frac{\pi(1-\eta_0)}{2\sqrt{(1-\eta_0^2)} - \eta_0 \cos^{-1}\eta_0} C(x) \tag{29}$$

$$D_3(x) = -\frac{\pi(1-\eta_0)^2}{(1+2\eta_0^2)\cos^{-1}\eta_0 - 3\eta_0\sqrt{(1-\eta_0^2)}} C(x). \tag{30}$$

The same relations are obtained from the condition that the spanwise velocity component, v_y, at the leading edge vanishes, which is a consequence of the condition of zero load at the leading edge. Within slender-wing theory, v_y is related to the spanwise distribution of the local chord load by:

$$\frac{v_y(x, y)}{V_0} = \pm\frac{1}{2}\frac{\partial\Gamma/V_0}{\partial y} = \pm\frac{1}{4}\frac{\partial L(x, y)}{\partial y}. \tag{31}$$

Applying the condition $v_y(x, \eta = 1) = 0$ to the functions $L_\nu(x, y)$ given by equations (20) to (22), leads to equations (28) to (30) and to equations (23) to (25).

Differentiating the distributions of the chord load given by equations (23) to (25), we obtain the following relations for the local load:

$$\begin{aligned} l_1(x, y) = {} & \frac{dC(x)}{dx} s(x) \frac{2}{\cos^{-1}\eta_0} \left\{ -\eta_0 \ln \frac{\left|\sqrt{(1-\eta^2)} - \sqrt{(1-\eta_0^2)}\right|}{\sqrt{(1-\eta^2)} + \sqrt{(1-\eta_0^2)}} + \right. \\ & \left. + \eta \ln \frac{\left|\eta_0\sqrt{(1-\eta^2)} - \eta\sqrt{(1-\eta_0^2)}\right|}{\eta_0\sqrt{(1-\eta^2)} + \eta\sqrt{(1-\eta_0^2)}} \right\} + \\ & + C(x) \frac{ds(x)}{dx} \frac{2}{\cos^{-1}\eta_0} \left\{ -\eta_0 \ln \frac{\left|\sqrt{(1-\eta^2)} - \sqrt{(1-\eta_0^2)}\right|}{\sqrt{(1-\eta^2)} + \sqrt{(1-\eta_0^2)}} \right\} + \\ & + C(x)s(x) \frac{d\eta_0(x)}{dx} \frac{2}{\cos^{-1}\eta_0\sqrt{(1-\eta_0^2)}} \left[-2\sqrt{(1-\eta^2)} - \right. \\ & - \left\{ \frac{\eta_0}{\cos^{-1}\eta_0} + \sqrt{(1-\eta_0^2)} \right\} \ln \frac{\left|\sqrt{(1-\eta^2)} - \sqrt{(1-\eta_0^2)}\right|}{\sqrt{(1-\eta^2)} + \sqrt{(1-\eta_0^2)}} + \\ & \left. + \frac{\eta}{\cos^{-1}\eta_0} \ln \frac{\left|\eta_0\sqrt{(1-\eta^2)} - \eta\sqrt{(1-\eta_0^2)}\right|}{\eta_0\sqrt{(1-\eta^2)} + \eta\sqrt{(1-\eta_0^2)}} \right]. \end{aligned} \tag{32}$$

$$l_2(x,y) = \frac{dC(x)}{dx}\, s(x)\, \frac{1}{\sqrt{(1-\eta_0^2)} - \eta_0 \cos^{-1}\eta_0} \left\{ 2\sqrt{(1-\eta_0^2)}\sqrt{(1-\eta^2)} + \right.$$

$$\left. + (\eta_0^2+\eta^2) \ln \frac{\left|\sqrt{(1-\eta^2)} - \sqrt{(1-\eta_0^2)}\right|}{\sqrt{(1-\eta^2)} + \sqrt{(1-\eta_0^2)}} - 2\eta_0\eta \ln \frac{\left|\eta_0\sqrt{(1-\eta^2)} - \eta\sqrt{(1-\eta_0^2)}\right|}{\eta_0\sqrt{(1-\eta^2)} + \eta\sqrt{(1-\eta_0^2)}} \right\} +$$

$$+ C(x)\, \frac{ds(x)}{dx}\, \frac{1}{\sqrt{(1-\eta_0^2)} - \eta_0 \cos^{-1}\eta_0} \left\{ 2\sqrt{(1-\eta_0^2)}\sqrt{(1-\eta^2)} + \right.$$

$$\left. + (\eta_0^2-\eta^2) \ln \frac{\left|\sqrt{(1-\eta^2)} - \sqrt{(1-\eta_0^2)}\right|}{\sqrt{(1-\eta^2)} + \sqrt{(1-\eta_0^2)}} \right\} +$$

$$+ C(x)s(x)\, \frac{d\eta_0(x)}{dx}\, \frac{1}{[\sqrt{(1-\eta_0^2)} - \eta_0 \cos^{-1}\eta_0]^2} \left[2\cos^{-1}\eta_0\sqrt{(1-\eta_0^2)}\sqrt{(1-\eta^2)} + \right.$$

$$+ \{2\eta_0\sqrt{(1-\eta_0^2)} + (\eta^2-\eta_0^2)\cos^{-1}\eta_0\} \ln \frac{\left|\sqrt{(1-\eta^2)} - \sqrt{(1-\eta_0^2)}\right|}{\sqrt{(1-\eta^2)} + \sqrt{(1-\eta_0^2)}} -$$

$$\left. - 2\eta\sqrt{(1-\eta_0^2)} \ln \frac{\left|\eta_0\sqrt{(1-\eta^2)} - \eta\sqrt{(1-\eta_0^2)}\right|}{\eta_0\sqrt{(1-\eta^2)} + \eta\sqrt{(1-\eta_0^2)}} \right] \qquad (33)$$

$$l_3(x,y) = \frac{dC(x)}{dx}\, s(x)\, \frac{4}{3[(1+2\eta_0^2)\cos^{-1}\eta_0 - 3\eta_0\sqrt{(1-\eta_0^2)}]} \times$$

$$\times \left[\{2(1-\eta^2)\cos^{-1}\eta_0 - 4\eta_0\sqrt{(1-\eta_0^2)}\}\sqrt{(1-\eta^2)} - \right.$$

$$- (\eta_0^3+3\eta_0\eta^2) \ln \frac{\left|\sqrt{(1-\eta^2)} - \sqrt{(1-\eta_0^2)}\right|}{\sqrt{(1-\eta^2)} + \sqrt{(1-\eta_0^2)}} +$$

$$\left. + (\eta^3+3\eta_0^2\eta) \ln \frac{\left|\eta_0\sqrt{(1-\eta^2)} - \eta\sqrt{(1-\eta_0^2)}\right|}{\eta_0\sqrt{(1-\eta^2)} + \eta\sqrt{(1-\eta_0^2)}} \right] +$$

$$+ C(x)\, \frac{ds(x)}{dx}\, \frac{4}{3[(1+2\eta_0^2)\cos^{-1}\eta_0 - 3\eta_0\sqrt{(1-\eta_0^2)}]} \times$$

$$\times \left[\{2(1+2\eta^2)\cos^{-1}\eta_0 - 4\eta_0\sqrt{(1-\eta_0^2)}\}\sqrt{(1-\eta^2)} + \right.$$

$$\left. + (3\eta_0\eta^2-\eta_0^3) \ln \frac{\left|\sqrt{(1-\eta^2)} - \sqrt{(1-\eta_0^2)}\right|}{\sqrt{(1-\eta^2)} + \sqrt{(1-\eta_0^2)}} - 2\eta^3 \ln \frac{\left|\eta_0\sqrt{(1-\eta^2)} - \eta\sqrt{(1-\eta_0^2)}\right|}{\eta_0\sqrt{(1-\eta^2)} + \eta\sqrt{(1-\eta_0^2)}} \right] +$$

$$+ C(x)s(x)\, \frac{d\eta_0(x)}{dx}\, \frac{4}{3[(1+2\eta_0^2)\cos^{-1}\eta_0 - 3\eta_0\sqrt{(1-\eta_0^2)}]^2} \times$$

$$\times \left[2\{\eta_0(1-\eta_0^2) + (1+2\eta_0^2-4\eta^2)\sqrt{(1-\eta_0^2)}\cos^{-1}\eta_0 - 4\eta_0(1-\eta^2)(\cos^{-1}\eta_0)^2\}\sqrt{(1-\eta^2)} + \right.$$

$$+ \{(5\eta_0^2-3\eta^2)\eta_0\sqrt{(1-\eta_0^2)} -$$

$$- (2\eta_0^4-6\eta_0^2\eta^2+3\eta_0^2+3\eta^2)\cos^{-1}\eta_0\} \ln \frac{\left|\sqrt{(1-\eta^2)} - \sqrt{(1-\eta_0^2)}\right|}{\sqrt{(1-\eta^2)} + \sqrt{(1-\eta_0^2)}} +$$

$$\left. + \{(4\eta^2-6\eta_0^2)\eta\sqrt{(1-\eta_0^2)} + (6-4\eta^2)\eta\,\eta_0\cos^{-1}\eta_0\} \ln \frac{\left|\eta_0\sqrt{(1-\eta^2)} - \eta\sqrt{(1-\eta_0^2)}\right|}{\eta_0\sqrt{(1-\eta^2)} + \eta\sqrt{(1-\eta_0^2)}} \right] \qquad (34)$$

The functions $l_\nu(x, y)$ are of the form:

$$l_\nu(x, y) = \frac{dC(x)}{dx} s(x) F_{1\nu}(\eta_0, \eta) + C(x) \frac{ds(x)}{dx} F_{2\nu}(\eta_0, \eta) + C(x)s(x) \frac{d\eta_0(x)}{dx} F_{3\nu}(\eta_0, \eta). \tag{35}$$

The functions $F_{n\nu}$ are zero for $\eta = 1$, i.e. $l_\nu\{x, y = s(x)\} = 0$ as required. The $F_{n\nu}(\eta_0, \eta)$ are finite for all values of η_0 and η, except for F_{21} and F_{31} which have logarithmically infinite values for $\eta = \eta_0$ as a consequence of the discontinuity in v_{z1} at $\eta = \eta_0$. The load distributions $l_1(x, y)$ (with the exception of the line $\eta = \eta_0$), $l_2(x, y)$ and $l_3(x, y)$ have, therefore, finite values over the whole wing surface if $dC(x)/dx$, $ds(x)/dx$ and $d\eta_0(x)/dx$ are finite over the wing.

The formulae for F_{n2} and F_{n3} are rather lengthy and of such a form that the numerical calculations have to be performed with a larger number of significant figures than required for the final result. We have, therefore, calculated the terms F_{n2} and F_{n3} for a few values of η_0 only and plotted charts for these terms, *see* Figs. 3 to 8.

The limits of $F_{n\nu}$ as $\eta_0 \to 1$ were required when drawing these charts. The limit of $l_\nu(x, y)$ for $\eta_0 \to 1$ is of further interest since we intend to take in some cases $\eta_0 = 1$ at the trailing edge to achieve elliptic distribution of the chord load. For $\sqrt{\{(1-\eta_0^2)/(1-\eta^2)\}} \to 0$, the numerator and the denominator in the $F_{n\nu}$ tend to zero. After some lengthy calculations we obtain for $\eta_0 \to 1$:

$$l_2(x, y) = \frac{dC(x)}{dx} s(x) 4\sqrt{(1-\eta^2)} + C(x) \frac{ds(x)}{dx} \frac{4}{\sqrt{(1-\eta^2)}} + C(x)s(x) \frac{d\eta_0(x)}{dx} \frac{8}{5} \frac{1}{\sqrt{(1-\eta^2)}} \tag{36}$$

$$l_3(x, y) = \frac{dC(x)}{dx} s(x) 4\sqrt{(1-\eta^2)} + C(x) \frac{ds(x)}{dx} \frac{4}{\sqrt{(1-\eta^2)}} + C(x)s(x) \frac{d\eta_0(x)}{dx} \frac{8}{7} \frac{1}{\sqrt{(1-\eta^2)}}. \tag{37}$$

For $\eta_0 \to 1$, $l_1(x, y)$ is infinite unless $d\eta_0(x)/dx$ is zero. If $\{d\eta_0(x)/dx\}_{\eta_0=1} = 0$, then $\{l_\nu(x, y)\}_{\eta_0=1}$ is, of course, the same for all ν.

3.4. *Chordwise Distribution of the Cross Load.*

As can be seen from equation (67) in Section 3.7, a knowledge of the chordwise distribution of the cross load, $L(x)$, is required to determine the wave drag at supersonic speed by the not-so-slender wing theory of Adams and Sears[9]. The chordwise distribution $L(x)$ can also be used to calculate the total lift on the wing. $L(x)$ is related to $l(x, y)$ by:

$$\begin{aligned} L(x) &= \int_{-s(x)}^{s(x)} l(x, y) dy \\ &= 2s(x) \int_0^1 l(x, \eta) d\eta. \end{aligned} \tag{38}$$

By equations (32) to (34) and (38)

$$\begin{aligned} L_1(x) = {} & \frac{dC(x)}{dx} s^2(x) \frac{2\pi}{\cos^{-1}\eta_0} \eta_0\sqrt{(1-\eta_0^2)} + C(x)s(x) \frac{ds(x)}{dx} \frac{4\pi}{\cos^{-1}\eta_0} \eta_0\sqrt{(1-\eta_0^2)} + \\ & + C(x)s^2(x) \frac{d\eta_0(x)}{dx} \frac{2\pi}{\cos^{-1}\eta_0\sqrt{(1-\eta_0^2)}} \{1 - 2\eta_0^2 - \eta_0 \cos^{-1}\eta_0\sqrt{(1-\eta_0^2)}\} \end{aligned} \tag{39}$$

$$\begin{aligned} L_2(x) = {} & \frac{dC(x)}{dx} s^2(x) \frac{2\pi\sqrt{(1-\eta_0^2)^3}}{3[\sqrt{(1-\eta_0^2)} - \eta_0 \cos^{-1}\eta_0]} + C(x)s(x) \frac{ds(x)}{dx} \frac{4\pi\sqrt{(1-\eta_0^2)^3}}{3[\sqrt{(1-\eta_0^2)} - \eta_0 \cos^{-1}\eta_0]} + \\ & + C(x)s^2(x) \frac{d\eta_0(x)}{dx} \frac{2\pi[(1+2\eta_0^2) \cos^{-1}\eta_0\sqrt{(1-\eta_0^2)} - 3\eta_0(1-\eta_0^2)]}{3[\sqrt{(1-\eta_0^2)} - \eta_0 \cos^{-1}\eta_0]^2} \end{aligned} \tag{40}$$

$$L_3(x) = \frac{dC(x)}{dx} s^2(x) \frac{\pi[3\cos^{-1}\eta_0 - (5\eta_0 - 2\eta_0^3)\sqrt{(1-\eta_0^2)}]}{3[(1+2\eta_0^2)\cos^{-1}\eta_0 - 3\eta_0\sqrt{(1-\eta_0^2)}]} +$$

$$+ C(x)s(x)\frac{ds(x)}{dx}\frac{2\pi[3\cos^{-1}\eta_0 - (5\eta_0 - 2\eta_0^3)\sqrt{(1-\eta_0^2)}]}{3[(1+2\eta_0^2)\cos^{-1}\eta_0 - 3\eta_0\sqrt{(1-\eta_0^2)}]} +$$

$$+ C(x)s^2(x)\frac{d\eta_0(x)}{dx} \times$$

$$\times \frac{4\pi[(\eta_0 - 4\eta_0^3)(1-\eta_0^2) + (1+3\eta_0^2+2\eta_0^4)\cos^{-1}\eta_0\sqrt{(1-\eta_0^2)} - 3\eta_0(\cos^{-1}\eta_0)^2]}{3[(1+2\eta_0^2)\cos^{-1}\eta_0 - 3\eta_0\sqrt{(1-\eta_0^2)}]^2}. \quad (41)$$

The limit of $L_1(x)$ as η_0 tends to one is infinite unless $d\eta_0/dx$ is zero. The limits of $L_2(x)$ and $L_3(x)$ for $\eta_0 \to 1$ are:

$$L_2(x) = \frac{dC(x)}{dx} s^2(x)\, 2\pi + C(x)s(x)\frac{ds(x)}{dx} 4\pi + C(x)s^2(x)\frac{d\eta_0(x)}{dx}\frac{8}{5}\pi \quad (42)$$

$$L_3(x) = \frac{dC(x)}{dx} s^2(x)\, 2\pi + C(x)s(x)\frac{ds(x)}{dx} 4\pi + C(x)s^2(x)\frac{d\eta_0(x)}{dx}\frac{8}{7}\pi. \quad (43)$$

The total load $\bar{L}_\nu(x)$ acting on the part of the wing in front of the station x = const. can be determined either by integrating the cross load $L_\nu(x)$ from the apex ($x = 0$) to the station x or by integrating the local chord load $L_\nu(x, y)$ with respect to y:

$$\bar{L}_\nu(x) = \int_0^x L_\nu(x')dx' = 2\int_0^{s(x)} L_\nu(x, y)dy. \quad (44)$$

We have obtained $\bar{L}_\nu(x)$ by integrating $L_\nu(x, y)$ and used the relation

$$L_\nu(x) = \frac{\partial}{\partial x}\bar{L}_\nu(x) \quad (45)$$

as a check of our various formulae. The result is:

$$\bar{L}_1(x) = C(x)s^2(x)2\pi \frac{\eta_0(x)\sqrt{\{1-\eta_0^2(x)\}}}{\cos^{-1}\eta_0(x)} \quad (46)$$

$$\bar{L}_2(x) = C(x)s^2(x)2\pi \frac{\sqrt{(1-\eta_0^2)^3}}{3[\sqrt{(1-\eta_0^2)} - \eta_0\cos^{-1}\eta_0]} \quad (47)$$

$$\bar{L}_3(x) = C(x)s^2(x)2\pi \frac{3\cos^{-1}\eta_0 - (5\eta_0 - 2\eta_0^3)\sqrt{(1-\eta_0^2)}}{6[(1+2\eta_0^2)\cos^{-1}\eta_0 - 3\eta_0\sqrt{(1-\eta_0^2)}]}. \quad (48)$$

Denoting by the suffix T the values at the trailing edge, the lift coefficient of the whole wing is given by relating the total load $\bar{L}(x_T)$ to the wing area, $2s_T\bar{c}$, ($\bar{c}$ is the geometric mean chord):

$$\bar{C}_L = \frac{\bar{L}(x_T)}{2s_T\bar{c}} = \frac{A}{4s_T^2}\bar{L}(x_T). \quad (49)$$

Thus:

$$\bar{C}_{L1} = \frac{\pi}{2}AC_T\frac{\eta_{0T}\sqrt{(1-\eta_{0T}^2)}}{\cos^{-1}\eta_{0T}} \quad (50)$$

$$\bar{C}_{L2} = \frac{\pi}{2}AC_T\frac{\sqrt{(1-\eta_{0T}^2)^3}}{3[\sqrt{(1-\eta_{0T}^2)} - \eta_{0T}\cos^{-1}\eta_{0T}]} \quad (51)$$

$$\bar{C}_{L3} = \frac{\pi}{2}AC_T\frac{3\cos^{-1}\eta_{0T} - (5\eta_{0T} - 2\eta_{0T}^3)\sqrt{(1-\eta_{0T}^2)}}{6[(1+2\eta_{0T}^2)\cos^{-1}\eta_{0T} - 3\eta_{0T}\sqrt{(1-\eta_{0T}^2)}]}. \quad (52)$$

The limit as $\eta_{0T} \to 1$ is, of course:

$$\bar{C}_L = \frac{\pi}{2} A C_T . \tag{53}$$

This is the lift coefficient of the flat wing set at an incidence $\alpha = C_T$ to the main stream if the flow separates only at the trailing edge. The ratio $\bar{C}_L/(\pi/2)AC_T$ of the lift coefficients for the cambered wing and for the flat wing is plotted in Fig. 9. That the total lift is fully determined by the shape of the wing at the trailing edge (C_T and η_{0T}) is a consequence of the assumptions of slender-wing theory.

3.5. *Spanwise Velocity Component.*

Our final aim is to calculate the pressure distribution on thick wings which have the warped wings of this report as mean surfaces. To determine the pressure distribution and the direction of the streamlines, we require the chordwise and spanwise velocity components on the thin wing.

The streamwise perturbation velocity, v_x, is given in terms of the local load coefficient:

$$\frac{v_{xU}(x, y)}{V_0} = \frac{1}{4} l(x, y) . \tag{54}$$

The spanwise perturbation velocity, v_y, which is induced on the thin warped wing is, within slender-wing theory, related to the spanwise distribution of the chord load, $L(x, y)$, by equation (31). We obtain by equations (23) to (25):

$$\frac{v_{y1}(x, y)}{V_0} = \pm\, C(x) \frac{1}{2 \cos^{-1}\eta_0} \ln \frac{|\eta_0\sqrt{(1-\eta^2)} - \eta\sqrt{(1-\eta_0^2)}|}{\eta_0\sqrt{(1-\eta^2)} + \eta\sqrt{(1-\eta_0^2)}} \tag{55}$$

$$\begin{aligned}\frac{v_{y2}(x, y)}{V_0} = \pm\, C(x) & \frac{1}{2[\sqrt{(1-\eta_0^2)} - \eta_0 \cos^{-1}\eta_0]} \times \\ & \times \left\{ \eta \ln \frac{|\sqrt{(1-\eta^2)} - \sqrt{(1-\eta_0^2)}|}{\sqrt{(1-\eta^2)} + \sqrt{(1-\eta_0^2)}} - \eta_0 \ln \frac{|\eta_0\sqrt{(1-\eta^2)} - \eta\sqrt{(1-\eta_0^2)}|}{\eta_0\sqrt{(1-\eta^2)} + \eta\sqrt{(1-\eta_0^2)}} \right\}\end{aligned} \tag{56}$$

$$\begin{aligned}\frac{v_{y3}(x, y)}{V_0} = \pm\, C(x) & \frac{1}{(1+2\eta_0^2)\cos^{-1}\eta_0 - 3\eta_0\sqrt{(1-\eta_0^2)}} \times \\ & \times \left\{ -2\eta \cos^{-1}\eta_0\sqrt{(1-\eta^2)} - 2\eta_0\eta \ln \frac{|\sqrt{(1-\eta^2)} - \sqrt{(1-\eta_0^2)}|}{\sqrt{(1-\eta^2)} + \sqrt{(1-\eta_0^2)}} + \right. \\ & \left. + (\eta^2+\eta_0^2) \ln \frac{|\eta_0\sqrt{(1-\eta^2)} - \eta\sqrt{(1-\eta_0^2)}|}{\eta_0\sqrt{(1-\eta^2)} + \eta\sqrt{(1-\eta_0^2)}} \right\} .\end{aligned} \tag{57}$$

For $\eta_0 \to 1$

$$\frac{v_{yp}(x, y)}{V_0} = \mp\, C(x) \frac{\eta}{\sqrt{(1-\eta^2)}} . \tag{58}$$

3.6. *Vortex Drag.*

Within slender-wing theory, the drag which occurs on a thin wing in non-viscous flow is only vortex drag, since lift-dependent wave drag is absent in this approximation, The vortex drag can be determined from the spanwise distribution of the chord load at the trailing edge and the downwash which the trailing vortices induce far downstream in the so-called Trefftz-plane:

$$\frac{D_v}{\frac{1}{2}\rho_0 V_0^2} = -\int_{-s_T}^{s_T} L(x = 1, y') \frac{1}{2} \frac{v_z(x = \infty, y')}{V_0} dy' . \tag{59}$$

Within the present approximation, the downwash in the Trefftz-plane is equal to the downwash at the trailing edge, so that:

$$\frac{D_{vv}}{\frac{1}{2}\rho_0 V_0^2} = s_T C_T \int_0^1 L_\nu(1, \eta')d\eta' + s_T D_{\nu T} \int_{\eta_{0T}}^1 \left(\frac{\eta' - \eta_{0T}}{1 - \eta_{0T}}\right)^{\nu-1} L_\nu(1, \eta')d\eta' . \tag{60}$$

Introducing the lift-dependent drag factor K:

$$K = \frac{\bar{C}_D}{\bar{C}_L^2/\pi A} = \frac{D_v}{\frac{1}{2}\rho_0 V_0^2} \frac{4\pi s_T^2}{\bar{L}^2}, \tag{61}$$

we obtain for the three cases considered the relations:

$$K_1 = \frac{-2 \ln \eta_{0T}}{1 - \eta_{0T}^2} \tag{62}$$

$$K_2 = \frac{-(9\eta_{0T}^2 - 3)(1 - \eta_{0T}^2) - 12\eta_{0T}^4 \ln \eta_{0T}}{2(1 - \eta_{0T}^2)^3} \tag{63}$$

$$K_3 = \frac{4}{5} \frac{\{-64\eta_{0T}^6 \ln \eta_{0T} + 15(\cos^{-1}\eta_{0T})^2 + (-54\eta_{0T} + 28\eta_{0T}^3 - 4\eta_{0T}^5)\sqrt{(1 - \eta_{0T}^2)} \cos^{-1}\eta_{0T} + + (51\eta_{0T}^2 - 68\eta_{0T}^4)(1 - \eta_{0T}^2)\}}{[3 \cos^{-1}\eta_{0T} - (5\eta_{0T} - 2\eta_{0T}^3)\sqrt{(1 - \eta_{0T}^2)}]^2} \tag{64}$$

For $\eta_{0T} \to 1$, $K_\nu \to 1$. To achieve minimum vortex drag, it is only necessary to have $\eta_0 = 1$ at the trailing edge, whereas elsewhere η_0 can be smaller than 1. This can easily be obtained on a wing with gothic planform. Values of K_ν are plotted in Fig. 10. The infinite value of K_1 for $\eta_{0T} \to 0$ is a consequence of

$$\lim_{\eta_{0T} \to 0} \left(\frac{\bar{C}_{L1}}{\eta_{0T}}\right) = \frac{\pi}{2} A C_T$$

{*see* equation (50)} and of

$$\frac{D_{v1}}{\frac{1}{2}\rho_0 V_0^2} = -C_T^2 s_T^2 \frac{2\pi}{(\cos^{-1}\eta_{0T})^2} \eta_{0T}^2 \ln \eta_{0T}$$

For all values of η_{0T} the vortex-drag factors K_2 and K_3 are smaller than the value $K = 2$ which is the limit of K for $\bar{C}_L \to 0$ for a flat plate with flow separation from all edges. Values of the drag factor which are of the same magnitude as the values of K_3 are obtained for the flat wing, if at all, only at relatively large $\bar{C}_L$ – values, which are much higher than those which lead to the optimum lift-drag ratio. But, on the other hand, the calculated results make it clear that a warping of the wing is only useful when the wing is carefully designed.

Let us consider wings with the same lift coefficient and the same vortex drag but with different spanwise downwash distributions ($\nu = 2$ and $\nu = 3$). For the quadratically varying downwash the shoulder position is farther inboard than for the linearly varying downwash, $\eta_{0T3} < \eta_{0T2}$. If we take from Fig. 10 values of $\eta_{0T\nu}$ which give the same value of K_ν, and determine from Fig. 2 for these $\eta_{0T\nu}$ the ratio $v_{z\nu}(1)/v_z(0)$, then we find that these are nearly equal. Fig. 9 shows that the values of $\bar{C}_L/(\pi/2)AC_T$ are also not very different. All this means that we obtain for the quadratically varying downwash a smoother section shape than with linearly varying downwash on wings with the same lift coefficient and the same vortex drag.

This fact poses the question, of why we have not gone further in our series of downwash distributions:

$$-\frac{v_z(x, y, 0)}{V_0} = C(x) + D_\nu(x)\left[\frac{|\eta| - \eta_0(x)}{1 - \eta_0(x)}\right]^{\nu-1}$$

$$\text{for } \eta_0(x) < |\eta| < 1.$$

The reason for not doing so is that we expect the amount of work involved to be disproportionate to possible gains.

3.7. *Wave Drag.*

In supersonic flow, a wave drag, D_w, arises in addition to the vortex drag, D_v. The total lift-dependent drag, D, is equal to the sum of vortex and wave drag:

$$D = D_v + D_w. \tag{65}$$

The wave drag can be determined by means of the 'equivalent lineal lift distributions' (*see* e.g. Refs. 11 and 12). The result can be expressed as a power series in βs_T, where

$$\beta = \sqrt{(M_0^2 - 1)} \tag{66}$$

and M_0 is the Mach number of the undisturbed flow. Adams and Sears[9] have determined the first term of this series. In our notation this term is:

$$\frac{D_w}{\frac{1}{2}\rho_0 V_0^2} = -\frac{\beta^2 s_T^2}{16\pi}\left[\int_{-1}^{+1}\int_{-1}^{+1} l(1, \eta)l(1, \eta') \ln|\eta - \eta'| d\eta' d\eta + \right.$$

$$+ \int_0^1\int_0^1 \frac{d}{dx}\left(\frac{L(x)}{s_T}\right)\frac{d}{dx'}\left(\frac{L(x')}{s_T}\right)\ln|x - x'| dx' dx -$$

$$\left. - 2\frac{L(1)}{s_T}\int_0^1 \frac{d}{dx}\left(\frac{L(x)}{s_T}\right)\ln(1-x)dx + \left(\frac{L(1)}{s_T}\right)^2\left\{-\frac{1}{2} + \ln\frac{\beta s_T}{2}\right\}\right] \tag{67}$$

where $l(1, \eta)$ is the load at the trailing edge and $L(x)$ the chordwise distribution of the cross load. For some special types of the functions $l(1, \eta)$ and $L(x)/s_T$, expressions in closed form for the double integrals of equation (67) are given in Appendix I.

For a wing with given geometry, the local load varies with increasing Mach number, i.e. increasing βs_T. Therefore, on a warped wing, designed by slender-wing theory so as to have zero load at the leading edge, the load will not be zero for finite values of βs_T. To produce zero load at a non-zero βs_T, a somewhat different wing shape is needed. To determine this, one might take the load distribution from slender-wing theory and calculate by linear theory the wing shape which produces that load distribution at a given βs_T. We do not intend to perform such a calculation but we can determine the lift-dependent drag which the slightly modified wing would have and use this as an approximation to the drag which the warped wing, designed for $\beta s_T = 0$, would have at a finite βs_T.

We insert the load distribution by slender-wing theory $l(x, y; \beta s_T = 0)$ into equation (67). This gives us an estimate of the wave drag of the known wing which is correct to the order of $\beta^4 s_T^4$ or $\beta^4 s_T^4 \ln \beta s_T$, because the difference between the load distributions determined for $\beta s_T = 0$ and $\beta s_T \neq 0$ is of the order $\beta^2 s_T^2$ or $\beta^2 s_T^2 \ln \beta s_T$. We are thus able to determine the wave drag due to lift to an absolute accuracy which is better than that for the wave drag due to thickness which we can determine easily only by slender-wing theory. The relative accuracy of the wave drag due to lift is of the same order as for the drag due to thickness.

For a given wing, the coefficients of the total lift and the vortex drag vary also with increasing βs_T. The correction terms to the results by slender-wing theory are of the order $\beta^2 s_T^2$. But the vortex-drag factor $\bar{C}_{Dv}/(C_L^2/\pi A)$ varies less with increasing βs_T than the vortex-drag coefficient. There are cases, as for instance the flat delta wing at incidence, for which the vortex-drag factor is independent of βs_T, i.e. equal to the value by slender-wing theory. For some other warped delta wings, see Appendix II, the error in the vortex-drag factor by slender-wing theory is only of the order $\beta^4 s_T^4$. We may thus expect to obtain a satisfactory estimate of the total lift-dependent drag factor for small finite βs_T by relating the sum of the vortex drag from slender-wing theory and the wave drag determined by equation (67) (from the load by slender-wing theory) to the term $\bar{C}_L^2/\pi A$ determined by slender-wing theory:

$$\frac{\bar{C}_D}{\bar{C}_L^2/\pi A} = \frac{\bar{C}_{Dv}(\beta s_T = 0) + \bar{C}_{Dw}\{l(x, y; \beta s_T = 0)\}}{[\bar{C}_L(\beta s_T = 0)]^2/\pi A} \tag{68}$$

4. *Calculated Examples.*

Some shapes of warped wings having zero load along the leading edge at the design $\bar{C}_L$ have already been given in Refs. 6 and 7 for the delta wing planform. The cambers considered are conical which in our case would mean straight shoulder lines {constant $\eta_0(x)$} and a straight centre section {constant $C(x)$}.

For the numerical examples of this report, we have chosen a wing with a gothic planform. The chosen aspect ratio is $0{\cdot}75$, i.e. $s_T/c_0 = 0{\cdot}25$. The design lift coefficient is $\bar{C}_L = 0{\cdot}1$. The spanwise downwash distribution outboard of the shoulder varies quadratically. Preference was given to the quadratically varying distribution since it produces smoother section shapes without any discontinuity in curvature. The centre section is straight. Since we have made the trailing edge straight, this implies that the inner part of the wing, $|y| < y_0$, is uncambered. The leading edge is not planar. If we had made it planar the spanwise sections would be cambered across the whole span.

The position of the shoulder, y_0, has been varied. We have chosen two shoulder lines. The first has $\eta_{0T} = 1$, which produces an elliptic spanwise distribution of the chord load at the trailing edge and thus a wing with minimum vortex drag. The corresponding wing shape has rather highly curved spanwise sections near the wing tips (*see* Fig. 13). The manufacture of this type of warped wings may be difficult since these highly curved parts occur at positions where with ordinary wing-thickness distributions the wing is relatively thin. It is also not quite certain whether it is justifiable to apply linear or slender-wing theory at these highly curved portions of the wing. We have, therefore, also considered wings with non-elliptic spanwise distribution of the chord load at the trailing edge ($\eta_{0T} \neq 1$). This means that the vortex-drag factor is larger than 1. For the chosen example $\eta_{0T} = 0{\cdot}8$ the factor is $1{\cdot}07$. We may, however, assume that a vortex-drag factor of $1{\cdot}07$ is still low compared with the drag factor on the flat wing with leading-edge separation, specially for the small value of the design lift coefficient chosen in our examples.

To simplify the geometry of the wing shapes, we have chosen two straight shoulder lines, one joining the apex to the tips and one joining the apex to the point at $0{\cdot}8$ semispan of the trailing edge. With these shoulder lines $d\eta_0(x)/dx$ at the trailing edge is finite. As a consequence the load at the trailing edge of these wings is finite, because it follows from equation (35) and Figs. 6 to 8 that the load at the trailing edge has a positive finite value if $\{ds(x)/dx\}_T > 0$, or $\{d\eta_0(x)/dx\}_T > 0$, or $\{dC(x)/dx\}_T = \{\partial^2 z(x, 0)/\partial x^2\}_T > 0$. For planforms with streamwise tips, such as the gothic planform, $\{ds(x)/dx\}_T = 0$.

(91392)

The considered chordwise variations of the position of the shoulder are such that the farther back on the wing the closer the shoulder is to the leading edge, as a consequence the spanwise sections are more highly curved near the trailing edge than near the apex. The least curved sections are, of course, obtained for wing (2) where the shoulder is everywhere more than 0·2 of the local span inboard of the leading edge.

Span- and chordwise distributions of the local load, span- and chordwise section shapes and spanwise velocity components for the two wings are plotted in Figs. 12 to 17.

The chordwise pressure distributions on the two wings show adverse gradients for most of the wing. So also do the spanwise distributions, if we consider a flow direction from the leading edge to the wing centre. We can, however, not yet decide whether the gradients are too large. The pressure distributions on thick warped wings, which have one of the two wings as their mean surface, depend at the small design $\bar{C}_L$ to a considerable degree on the thickness distribution. As a first step, to find out whether the pressure gradients are too large, we have to determine from the span- and chordwise velocity components on the thick warped wing the direction of the stream lines and then the pressure gradients along the stream lines. This has not yet been done. But we know that most thickness distributions have a beneficial effect on the pressure distribution, since thickness alone produces a positive pressure coefficient near the leading edge. We may, however, recall that the magnitude of the pressure coefficient near the leading edge, calculated by linear theory, is somewhat doubtful (*see* e.g. Ref. 13). There exist thickness distributions which give also farther inboard a beneficial reduction of the chordwise and spanwise pressure gradients (*see* e.g. Refs. 13 and 14). Let us choose e.g. a thickness distribution which has a cross-sectional area distribution corresponding to the distribution V of Ref. 14, cross-sections of diamond shape and a centre section with a thickness-chord radio of 0·08. Superposing this thickness distribution on the mean surface given by wing (2) we obtain, at the design $\bar{C}_L$, chord- and spanwise pressure distributions which are almost free of adverse gradients.

For wing (1) we have determined the wave drag for non-zero βs_T by equation (67). For wing (1) $\eta_{0T} = 1$ and therefore the load distribution at the trailing edge $l(1, \eta)$ is of the type given by equation (69) in Appendix I, so that the first double integral in equation (67) can be evaluated explicitly by equation (71). For the cases with $\eta_{0T} \neq 1$ and $\{d\eta_0(x)/dx\}_T \neq 0$ {as e.g. wing (2)}, no explicit value for the integral has yet been found.

The value of the second double integral in equation (67) can be estimated by means of equation (73) of Appendix I. For the wings considered, the chordwise distribution of the span load $L(x)$ (*see* Fig. 18) is such that it can be approximated by a polynomial in x, equation (72). The resulting drag factor, equation (68) is given by $1 + \beta^2 s_T^2(1{\cdot}83 - 0{\cdot}08 \ln \beta s_T)$; for the flat wing the factor is $1 + \beta^2 s_T^2 \times 2{\cdot}33$. For wing (2) {for which we have not yet calculated the first double integral in equation (67) since $\eta_{0T} \neq 1$}, we can assume that the wave drag is of the same order as that for wing (1), since the chordwise distributions of the span load are very similar (*see* Fig. 18).

We have plotted in Fig. 19 also the drag factor for the plane gothic wing with trailing-edge separation only, i.e. assuming at $\beta s_T = 0$ a drag factor of 1. The wave drag on the flat wing is 17 per cent higher than the minimum wave drag for very narrow wings, which is obtained with an elliptic chordwise load distribution (R. T. Jones' 'lower bound').

With the irrelevant exception of very small βs_T, wing (1) has a smaller drag than the plane gothic wing; the values are near R. T. Jones' 'lower bound'. The elliptic chordwise loading is only the optimum for small values of βs_T. It is therefore theoretically possible to obtain for larger values of

βs_T for some cases {as wing (1)} a smaller drag factor than R. T. Jones' lower bound for narrow wings.

5. *Conclusions.*

The aim of this report is to design warped slender wings such that the calculated flow represents a realistic physical flow and that low values of the drag due to lift are achieved. Existing methods of designing warped wings which have, at the design $\bar{C}_L$, zero load along the leading edge are usually restricted to wings of delta planform and to conical flow. In this report, the problem has, therefore, been extended in three directions:

(i) Slender wings with pointed nose and straight trailing edge but otherwise arbitrary planform are treated.

(ii) The basic wing can be plane or curved, i.e. the centre section can possess an arbitrary chordwise curvature.

(iii) The spanwise downwash distribution can vary along the chord, e.g. on a delta wing with straight centre section the flow need not be conical.

With the present method one can satisfy a variety of conditions, though not all at once:

(i) It is possible to choose for a given thickness distribution a mean surface so that no adverse pressure gradients or a limited adverse pressure gradient (if one knew what is desirable) occurs on the wing.

(ii) One can choose the amount of the rise in pressure required from the flow behind the wing to return to the free-stream pressure.

(iii) Low vortex drag, even the minimum value, can be obtained.

(iv) Low wave drag due to lift can be obtained.

(v) A spanwise section shape, in particular the position of the shoulder, could be chosen as to ensure that in off-design conditions the primary separation from the leading edge dominates the flow field, if one knew the geometric requirements.

(vi) One can choose from a variety of geometrical shapes to meet other than aerodynamic requirements.

(vii) One can choose the position of the centre of pressure at the design $\bar{C}_L$.

(viii) One can choose a compromise between the various requirements.

The calculations are based on slender-wing theory except for the wave drag which is determined from an approximate relation derived by the not-so-slender wing theory of Adams and Sears[9]. By making use of calculations by Lance[15], who has applied linear supersonic theory to warped wings of delta planform, it is shown that the value of the slenderness parameter βs_T, up to which slender-wing theory is applicable, depends to a large extent on the chordwise curvature. However, the drag factors, determined by the approximate relation, are reasonably accurate for $\beta s_T < 0{\cdot}4$.

The theory, as available at the present, cannot yet give us an answer to the following questions:

(i) What is the range of the validity of slender-wing theory for warped wings of other than delta planform? Is the surface slope near the leading edge on the wings, as designed in this report, small enough to allow the application of linear theory?

(ii) How do viscous effects alter the calculated pressure distribution and the drag at the design $\bar{C}_L$?

(iii) How do the wings behave at off-design conditions?

(a) Does the flow separation from the leading edge dominate the flow field?

(b) Is it more profitable to cruise at the $\bar{C}_L$ where the attachment line is along the leading edge or at a slightly higher $\bar{C}_L$ – value? The answer to this question will determine the value of the $\bar{C}_L$ for which the warped wing ought to be designed.

(c) How do the warped wings behave at high lift and under asymmetric conditions, e.g. yaw?

(d) How does the centre of pressure vary with $\bar{C}_L$? Is there a need for a special study of warped wings with fixed centre of pressure?

It is hoped that answers to at least some of these questions will be given by experiments now planned.

LIST OF SYMBOLS

x, y, z — Cartesian co-ordinates; origin at the wing apex; x along the free-stream direction, y spanwise, z positive upwards; all lengths are made dimensionless with the root chord

$z(x, y)$ — Ordinate of wing surface

$z_T = z(1, 0)$ — Ordinate of the trailing edge

$c_0 = 1$, chord of the centre section

$\bar{c}$ — Geometric mean chord

$s(x)$ — Local semispan

s_T — Semispan at the trailing edge

y_0 — Spanwise position of the 'shoulder' where the spanwise curvature begins

$\eta = \dfrac{y}{s(x)}$, non-dimensional spanwise ordinate

$\eta_0 = \dfrac{y_0}{s(x)}$, non-dimensional spanwise position of the 'shoulder'

η_{0T} — Value of η_0 at the trailing edge

$A = \dfrac{2s_T}{\bar{c}}$, aspect ratio

V_0 — Velocity of the undisturbed flow

v_x, v_y, v_z — Components of the perturbation velocity

M_0 — Mach number of the undisturbed flow

$\beta = \sqrt{(M_0^2 - 1)}$

$C(x) = -\dfrac{\partial z(x, 0)}{\partial x} = -\dfrac{v_z(x, 0, 0)}{V_0}$, downwash at the centre section

C_T — Downwash at the trailing edge of the centre section

$D_\nu(x)$ — Parameter in the downwash equation, *see* equation (6)

$l(x, y)$ — Local load coefficient

$L(x, y) = \displaystyle\int_{x_{\mathrm{LE}}(y)}^{x} l(x', y)dx'$, local chord load

$L(x) = \displaystyle\int_{-s(x)}^{s(x)} l(x, y')dy'$, cross load

$\bar{L}(x) = \displaystyle\int_0^x L(x')dx' = \int_{-s(x)}^{s(x)} L(x, y)dy$, local total load

$\bar{C}_L$	Total lift coefficient
D_v	Vortex drag
D_w	Lift-dependent wave drag
D	Total lift-dependent drag
$\bar{C}_{Dv}$	Vortex-drag coefficient
$\bar{C}_{Dw}$	Wave-drag coefficient
$\bar{C}_D$	Total lift-dependent drag coefficient
$K = \dfrac{\bar{C}_D}{\bar{C}_L^2/\pi A}$	lift-dependent drag factor
ϕ	Perturbation velocity potential in plane $z = 0$
$\Delta\phi$	Difference of ϕ on upper and lower surface
Γ	Circulation
F_{nv}	Factors in the loading equation, *see* equation (35)

Suffices

v	Suffix which characterises the type of the spanwise distribution of the downwash, *see* equation (6)
T	Trailing edge

REFERENCES

No.	Author(s)	Title, etc.
1	E. C. Maskell	Flow separation in three dimensions. A.R.C. 18 063. November, 1955.
2	D. Küchemann	A non-linear lifting-surface theory for wings of small aspect ratio with edge separations. A.R.C. 17 769. April, 1955.
3	J. Weber	Some effects of flow separation on slender delta wings. A.R.C. 18 073. November, 1955.
4	K. W. Mangler and J. H. B. Smith	Calculation of the flow past slender delta wings with leading edge separation. *Proc. Roy. Soc.* A, Vol. 251, pp. 200 to 217. 1959.
5	J. H. B. Smith	A theory of the separated flow from the curved leading edge of a slender wing. A.R.C. R. & M. 3116. November, 1957.
6	G. G. Brebner	Some simple conical camber shapes to produce low lift-dependent drag on a slender delta wing. A.R.C. C.P. 428. September, 1957.
7	J. H. B. Smith and K. W. Mangler	The use of conical camber to produce flow attachment at the leading edge of a delta wing to minimise lift-dependent drag at sonic and supersonic speeds. A.R.C. R. & M. 3289. September, 1957.
8	R. T. Jones	The minimum drag of thin wings in frictionless flow. *J. Ae. Sci.*, Vol. 18, p. 75. February, 1951.
9	Mac C. Adams and W. R. Sears..	Slender-body theory—Review and extension. *J. Ae. Sci.*, Vol. 20, p. 85. February, 1953.
10	E. J. Watson	Calculation of the circulation from the downwash. Appendix to 'Tables of Multhopp and other functions for use in lifting-line and lifting-plane theory' by V. M. Falkner. A.R.C. R. & M. 2593. February, 1948.
11	R. T. Jones	Theoretical determination of the minimum drag of airfoils at supersonic speeds. *J. Ae. Sci.*, Vol. 19, p. 813. December, 1952.
12	E. W. Graham, P. A. Lagerstrom, B. J. Beane and R. M. Licher.	A theoretical investigation of the drag of generalised aircraft configurations in supersonic flow. Douglas-Aircraft Company Report SM-19181. July, 1955.
13	J. Weber	Slender delta wings with sharp edges at zero lift. A.R.C. 19 549. May, 1957.
14	W. T. Lord and G. G. Brebner ..	Supersonic flow past slender pointed wings with 'similar' cross sections at zero lift. *Aero. Quart.*, Vol. 10, p. 79. 1959.
15	G. N. Lance	The delta wing in a non-uniform supersonic stream. *Aero. Quart.*, Vol. 5, p. 55. May, 1954.

APPENDIX I

Some Special Integrals

For

$$l(1, \eta) = a\sqrt{(1-\eta^2)} + b\,\frac{1}{\sqrt{(1-\eta^2)}} \tag{69}$$

the double integral

$$\mathrm{I} = \int_{-1}^{+1}\int_{-1}^{+1} l(1, \eta) l(1, \eta') \ln|\eta - \eta'|\, d\eta' d\eta \tag{70}$$

can be evaluated in closed form. We consider first the function

$$\mathrm{I}_1(\eta) = \int_{-1}^{+1}\left[a\sqrt{(1-\eta'^2)} + b\,\frac{1}{\sqrt{(1-\eta'^2)}}\right]\ln|\eta - \eta'|\, d\eta' .$$

Its derivative with respect to η

$$\frac{dI_1(\eta)}{d\eta} = \int_{-1}^{+1}\left[a\sqrt{(1-\eta'^2)} + b\,\frac{1}{\sqrt{(1-\eta'^2)}}\right]\frac{d\eta'}{\eta - \eta'}$$

can be determined explicitly. We introduce

$$\eta' = \cos\vartheta$$

$$\eta = \cos\phi$$

then

$$\frac{dI_1(\eta)}{d\eta} = \int_0^{\pi} \frac{a\sin^2\vartheta + b}{\cos\phi - \cos\vartheta}\, d\vartheta$$

$$= a\pi\cos\phi$$

$$= a\pi\eta .$$

Therefore

$$I_1(\eta) = a\,\frac{\pi}{2}\,\eta^2 + I_1(\eta = 0)$$

$$I_1(\eta = 0) = 2\int_0^1\left[a\sqrt{(1-\eta'^2)} + b\,\frac{1}{\sqrt{(1-\eta'^2)}}\right]\ln\eta' d\eta'$$

$$= -\pi\left(\frac{a}{4} + \frac{a}{2}\ln 2 + b\ln 2\right)$$

$$I_1(\eta) = \pi\left(\frac{a}{2}\,\eta^2 - \frac{a}{4} - \frac{a}{2}\ln 2 - b\ln 2\right).$$

Inserting this expression of $I_1(\eta)$ into equation (70) we get finally

$$\int_{-1}^{+1}\int_{-1}^{+1}\left[a\sqrt{(1-\eta^2)} + b\,\frac{1}{\sqrt{(1-\eta^2)}}\right]\left[a\sqrt{(1-\eta'^2)} + b\,\frac{1}{\sqrt{(1-\eta'^2)}}\right]\ln|\eta - \eta'|\, d\eta' d\eta =$$

$$-\pi^2\left[\frac{a^2}{16} + \left(\frac{a}{2} + b\right)^2\ln 2\right]. \tag{71}$$

For a polynomial expression of $L(x)$

$$\frac{L(x)}{s_T} = cx + dx^2 + ex^3 + fx^4 + gx^5 \tag{72}$$

the double integral

$$\int_0^1 \int_0^1 \frac{d}{dx}\left(\frac{L(x)}{s_T}\right) \frac{d}{dx'}\left(\frac{L(x')}{s_T}\right) \ln|x - x'|\, dx'dx$$

can be evaluated in closed form. The result is:

$$\int_0^1 \int_0^1 \frac{d}{dx}\left(\frac{L(x)}{s_T}\right) \frac{d}{dx'}\left(\frac{L(x')}{s_T}\right) \ln|x - x'|\, dx'dx =$$

$$-\frac{3}{2}c^2 - 3cd - \frac{35}{12}ce - \frac{17}{6}cf - \frac{497}{180}cg - \frac{7}{4}d^2 - \frac{11}{3}de -$$

$$-\frac{67}{18}df - \frac{56}{15}dg - 2e^2 - \frac{25}{6}ef - \frac{1021}{240}eg - \frac{53}{24}f^2 - \frac{137}{30}fg - \frac{143}{60}g^2 \tag{73}$$

$$\int_0^1 \int_0^1 \frac{d}{dx}\left(\frac{L(x)}{s_T}\right) \frac{d}{dx'}\left(\frac{L(x')}{s_T}\right) \ln|x - x'|\, dx'dx -$$

$$-2\frac{L(1)}{s_T}\int_0^1 \frac{d}{dx}\left(\frac{L(x)}{s_T}\right) \ln(1-x)dx - \frac{1}{2}\left(\frac{L(1)}{s_T}\right)^2 =$$

$$cd + \frac{7}{4}ce + \frac{7}{3}cf + \frac{101}{36}cg + \frac{3}{4}d^2 + 2de +$$

$$+\frac{22}{9}df + \frac{17}{6}dg + \frac{7}{6}e^2 + \frac{8}{3}ef + \frac{143}{48}eg + \frac{35}{24}f^2 + \frac{19}{6}fg + \frac{101}{60}g^2. \tag{74}$$

APPENDIX II

Comparison of Results Obtained by Slender-Wing Theory, Not-So-Slender-Wing Theory and by Linear Theory

To investigate the range of validity of slender-wing theory for lifting wings, we make use of calculations made by Lance[15] for warped wings of delta planform, applying linear supersonic theory. No such calculations for wings with highly swept leading edges but other than delta planform are known to the author. We shall compare some of the results of Ref. 15 with those by slender-wing theory.

Let us consider the cases where the downwash is of the type:

$$-v_z = v_n x^n .$$

These downwash distributions are different from those in the present report since they lead to wing shapes which have infinite load at the leading edges. We quote the load distributions from Ref. 15. In our notation:

$-v_z = v_0$:

$$l(x, y) = 4s \frac{v_0}{V_0} \frac{1}{E} \frac{1}{\sqrt{(1-\eta^2)}} . \tag{75}$$

$-v_z = v_1 x$:

$$l(x, y) = 4s \frac{v_1}{V_0} \frac{1-\beta^2 s^2}{(1-2\beta^2 s^2)E + \beta^2 s^2 K} \frac{x(2-\eta^2)}{\sqrt{(1-\eta^2)}} . \tag{76}$$

$-v_z = v_2 x^2$:

$$l(x, y) = 4s \frac{v_2}{V_0} \frac{x^2(c_1 - c_2\eta^2)}{\sqrt{(1-\eta^2)}} \tag{77}$$

where:

$$c_1 = \frac{4(3-5\beta^2 s^2+\beta^4 s^4)E - 2\beta^2 s^2(3-5\beta^2 s^2)K}{(4-19\beta^2 s^2+4\beta^4 s^4)E^2 + 8\beta^2 s^2(1+\beta^2 s^2)KE - 5\beta^4 s^4 K^2} \tag{78}$$

$$c_2 = \frac{2(4-7\beta^2 s^2+\beta^4 s^4)E - 4\beta^2 s^2(1-2\beta^2 s^2)K}{(4-19\beta^2 s^2+4\beta^4 s^4)E^2 + 8\beta^2 s^2(1+\beta^2 s^2)KE - 5\beta^4 s^4 K^2} . \tag{79}$$

$-v_z = v_3 x^3$:

$$l(x, y) = 4s \frac{v_3}{V_0} \frac{x^3(c_3 - c_4\eta^2 - c_5\eta^4)}{\sqrt{(1-\eta^2)}} \tag{80}$$

$$c_3 = \frac{8(1-\beta^2 s^2)}{D} [(6-15\beta^2 s^2+5\beta^4 s^4-4\beta^6 s^6)E - \beta^2 s^2(3-9\beta^2 s^2-2\beta^4 s^4)K] \tag{81}$$

$$c_4 = \frac{2(1-\beta^2 s^2)}{D} [(18-51\beta^2 s^2+\beta^4 s^4-8\beta^6 s^6)E - \beta^2 s^2(9-45\beta^2 s^2-4\beta^4 s^4)K] \tag{82}$$

$$c_5 = \frac{2(1-\beta^2 s^2)}{D} [(3+7\beta^2 s^2-2\beta^4 s^4)E - \beta^2 s^2(9-\beta^2 s^2)K] \tag{83}$$

$$D = (12-119\beta^2 s^2+151\beta^4 s^4-64\beta^6 s^6+32\beta^8 s^8)E^2 + \\ + 2\beta^2 s^2(24-5\beta^2 s^2-15\beta^4 s^4-16\beta^6 s^6)KE - \beta^4 s^4(27-31\beta^2 s^2-8\beta^4 s^4)K^2 . \tag{84}$$

E and K are the complete elliptic integrals of the modulus k, with $k^2 = 1 - k'^2 = 1 - \beta^2 s^2$, and s is the ratio between the semispan at the trailing edge and the root chord.

The load distributions of slender-wing theory are obtained by putting $\beta s = 0$. In Figs. 20, 21 we have plotted the ratio between the values of the local load obtained by slender-wing theory, $l(x, y; \beta s = 0)$, and by the more exact theory, $l(x, y)$. For the constant and the linearly varying downwash distributions ($n = 0, 1$), this ratio is the same for all points on the wing, but for the two other cases ($n = 2, 3$) it varies somewhat with the spanwise position of the point considered, *see* Fig. 21. In Fig. 20 we have compared the values of the load at the centre section. It has been suggested in Ref. 13 that for sharp edged delta wings the pressure distribution due to wing thickness can be estimated fairly well by slender-wing theory for values of βs smaller than about $0 \cdot 3$ (except very close to the leading edge where linear theory and slender-wing theory fail). Fig. 20 shows that for the pressure distributions due to camber the agreement between the exact results and those calculated by slender-wing theory depends noticeably on the wing shape. The error is largest for the wing with the largest value of the maximum curvature of the chordwise sections, i.e. $[\partial^2 z(x, y)/\partial x^2]_{\max}$. This was to be expected since with relatively large values of the maximum of the chordwise curvature and correspondingly large variations of the chordwise curvature the assumptions of slender-wing theory are less justified.

Generalizing the present results, we may expect that for wings with relatively small values of $[\partial^2 z(x, y)/\partial x^2]_{\max}$ slender-wing theory gives reasonable estimates for values of βs of about $0 \cdot 3$, but for wings with not so small values of $[\partial^2 z(x, y)/\partial x^2]_{\max}$ a value of βs smaller than $0 \cdot 3$ is required to obtain a sufficiently accurate estimate of the load distribution.

Using the exact load distributions of Ref. 15, we can also check the accuracy of the drag values obtained from the approximate relation, equation (68), which was derived by the not-so-slender wing theory of Adams and Sears. From the exact load distributions we have determined the total lift coefficient, $\bar{C}_L$, and the coefficient of the total lift-dependent drag, $\bar{C}_D$, taking account of the chordwise component of the suction force, $\bar{C}_{Sx}$:

$$\bar{C}_D = \bar{C}_{DP} - \bar{C}_{Sx}. \tag{85}$$

The coefficient of the local pressure drag at the section y, $C_{DP}(y)$, is given by

$$C_{DP}(y)\, c(y) = - \int_{x_{\mathrm{LE}}(y)}^{1} \frac{\partial z(x, y)}{\partial x}\, l(x, y) dx. \tag{86}$$

If the load distribution near the leading edge is expressed in the form:

$$l(x, y) = \frac{4}{\sqrt{(2\xi)}} F \tag{87}$$

where

$$\xi = \frac{x - x_{\mathrm{LE}}}{c(y)},$$

the chordwise component of the local suction force is:

$$C_{Sx}(y) = - \pi F^2 \sqrt{(\tan^2 \phi_{\mathrm{LE}} - \beta^2)} \tag{88}$$

and in the special case of a delta wing:

$$C_{Sx}(y) = - \pi s F^2 \sqrt{(1 - \beta^2 s^2)}. \tag{89}$$

Finally, we determine the drag factor, $\bar{C}_D/\bar{C}_L{}^2/\pi A$. The results are:

$-v_z = v_0$:

$$\frac{\bar{C}_D}{\bar{C}_L{}^2/\pi A} = 2E - \sqrt{(1-\beta^2 s^2)} \tag{90}$$

$-v_z = v_1 x$:

$$\frac{\bar{C}_D}{\bar{C}_L{}^2/\pi A} = \frac{3[(1-2\beta^2 s^2)E + \beta^2 s^2 K]}{2(1-\beta^2 s^2)} - \frac{1}{2}\sqrt{(1-\beta^2 s^2)} \tag{91}$$

$-v_z = v_2 x^2$:

$$\frac{\bar{C}_D}{\bar{C}_L{}^2/\pi A} = \frac{16}{3}\frac{(2c_1 - c_2) - \sqrt{(1-\beta^2 s^2)}\,(c_1 - c_2)^2}{(2c_1 - c_2)^2} \tag{92}$$

$-v_z = v_3 x^3$:

$$\frac{\bar{C}_D}{\bar{C}_L{}^2/\pi A} = \frac{40(11c_3 - 4c_4) - 4\sqrt{(1-\beta^2 s^2)}\,(5c_3 - 4c_4)^2}{(11c_3 - 4c_4)^2}. \tag{93}$$

Using the load distribution derived by slender-wing theory, $l(x, y;\ \beta s = 0)$, we have determined the wave drag by equation (67) and related it to the value of $\bar{C}_L{}^2/\pi A$ for $\beta s = 0$.

For the present examples the spanwise distribution of the chord load for $\beta s = 0$ is elliptic and thus

$$\left(\frac{\bar{C}_D}{\bar{C}_L{}^2/\pi A}\right)_{\beta s=0} = 1.$$

The approximation to the drag factor for small βs obtained from equation (68) is thus for

$-v_z = v_0$:

$$\frac{\bar{C}_D}{\bar{C}_L{}^2/\pi A} = 1 + \beta^2 s^2[2\ln 2 - \ln \beta s] \tag{94}$$

$-v_z = v_1 x$:

$$\frac{\bar{C}_D}{\bar{C}_L{}^2/\pi A} = 1 + \beta^2 s^2\left[\frac{9}{2}\ln 2 - \frac{13}{8} - \frac{9}{4}\ln \beta s\right] \tag{95}$$

$-v_z = v_2 x^2$:

$$\frac{\bar{C}_D}{\bar{C}_L{}^2/\pi A} = 1 + \beta^2 s^2\left[8\ln 2 - \frac{53}{12} - 4\ln \beta s\right] \tag{96}$$

$-v_z = v_3 x^3$:

$$\frac{\bar{C}_D}{\bar{C}_L{}^2/\pi A} = 1 + \beta^2 s^2\left[\frac{25}{2}\ln 2 - \frac{821}{96} - \frac{25}{4}\ln \beta s\right]. \tag{97}$$

Expressing the exact results for the drag factor, equations (90) to (93), as a power series in βs, we obtain for the first terms the same relations as in the approximations, equations (94) to (97). This is a consequence of the fact that for the present examples the power series for the vortex-drag factor $\bar{C}_{Dv}/(\bar{C}_L{}^2/\pi A)$ does not contain a term of order $\beta^2 s^2$. Fig. 22 gives a comparison of the exact and approximate values of the drag factor. The accuracy of the results obtained by the approximate formula, equation (68), is sufficient for $\beta s < 0{\cdot}3$ for all examples.

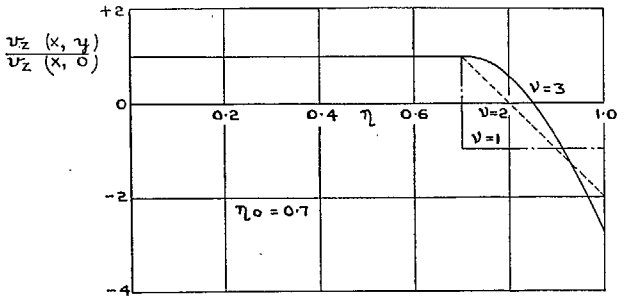

FIG. 1. Considered types of spanwise downwash distributions.

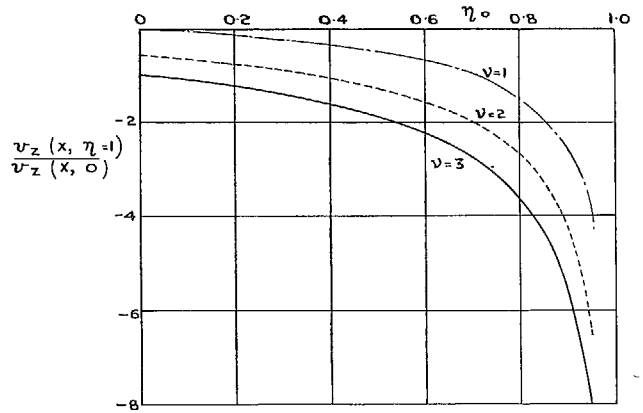

FIG. 2. Ratio between the downwashes at the leading edge and in the wing centre.

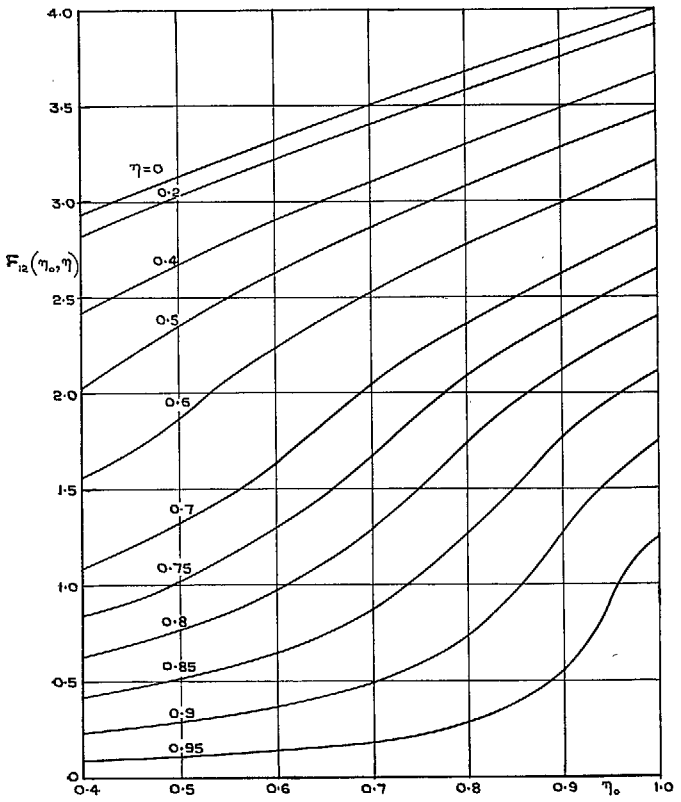

FIG. 3. Factor for $\{dC(x)/dx\}s(x)$ in $l_2(x, y)$, *see* equation (35).

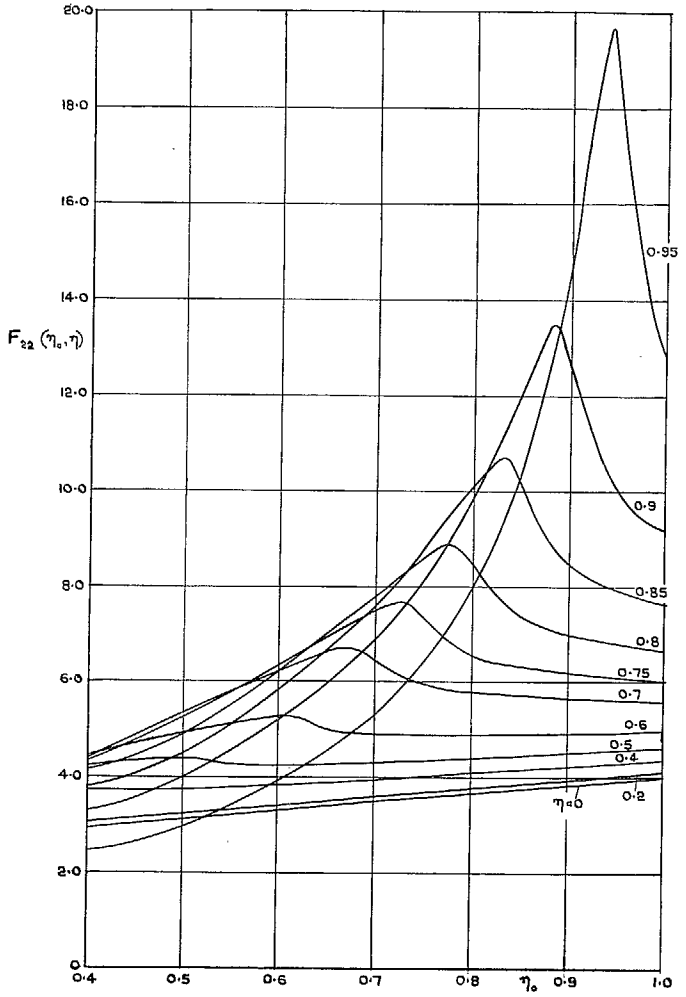

FIG. 4. Factor for $C(x)\ \{ds(x)/dx\}$ in $l_2(x, y)$, *see* equation (35).

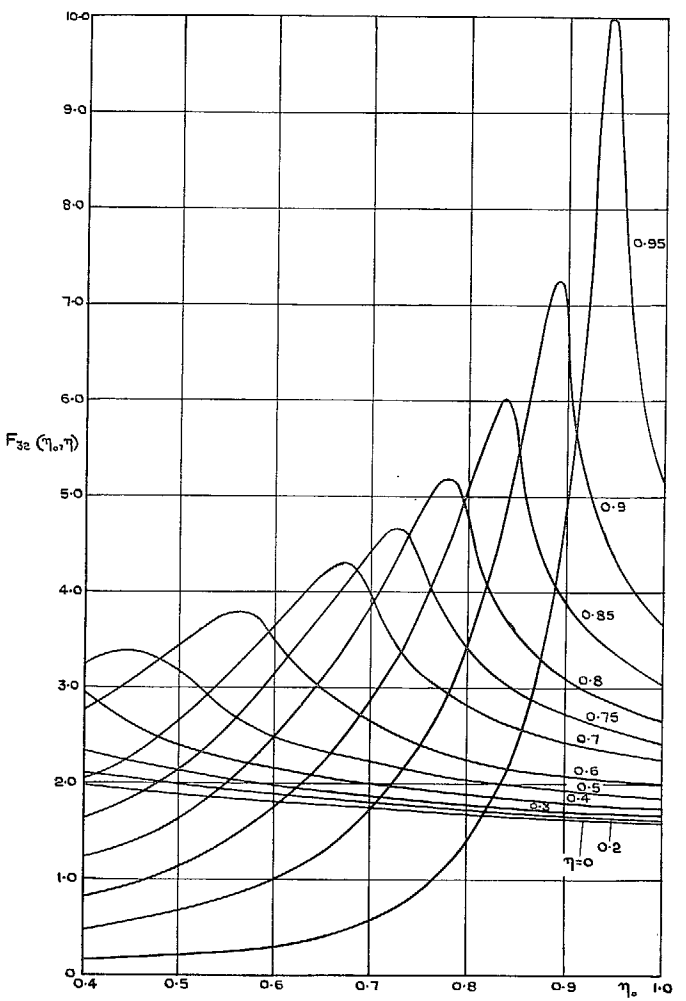

FIG. 5. Factor for $C(x)s(x)\ \{d\eta_0(x)/dx\}$ in $l_2(x, y)$, *see* equation (35).

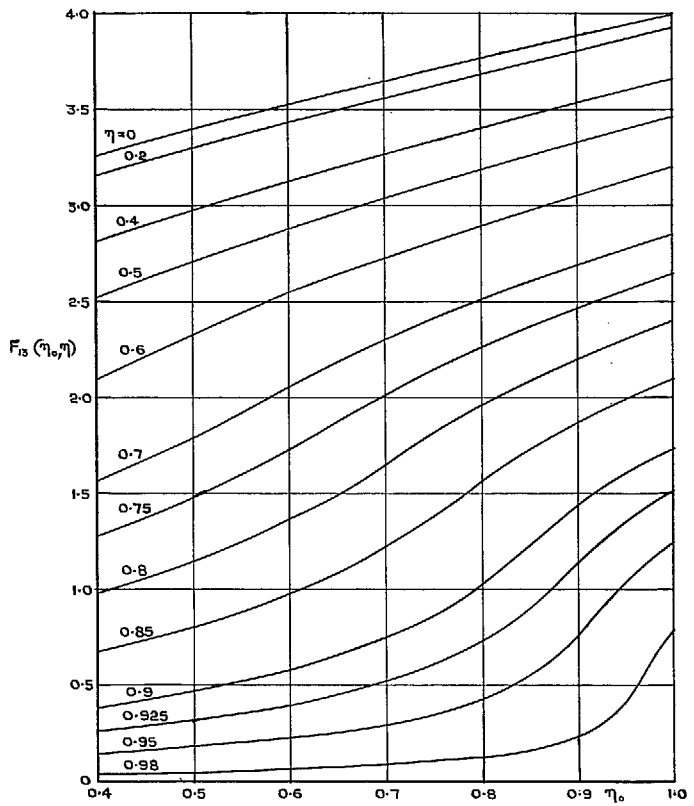

FIG. 6. Factor for $\{dC(x)/dx\}s(x)$ in $l_3(x, y)$, *see* equation (35).

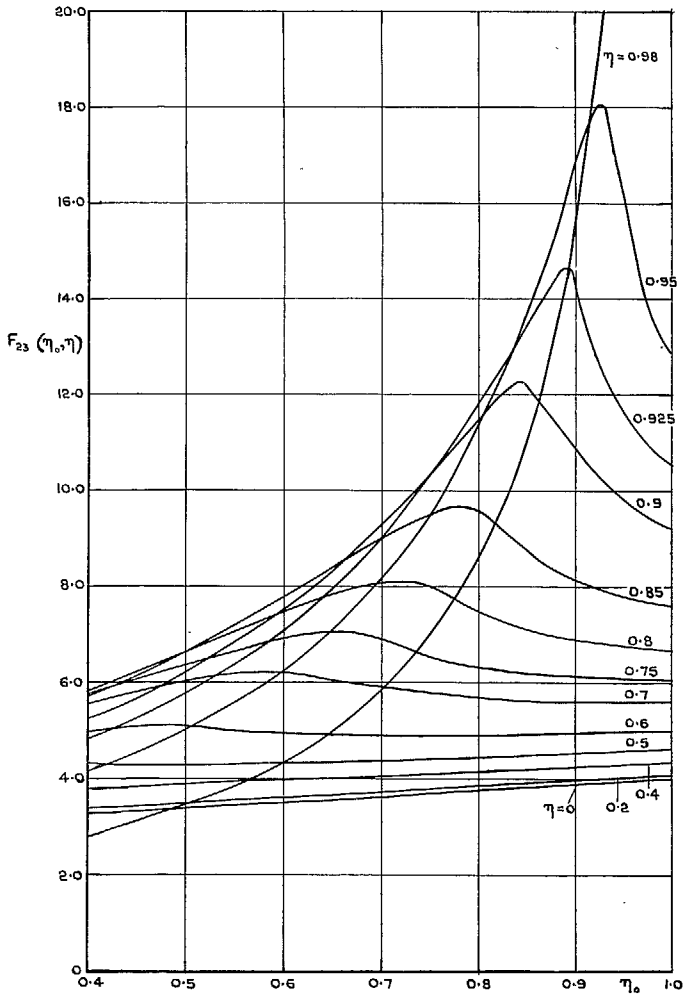

FIG. 7. Factor for $C(x)\ \{ds(x)/dx\}$ in $l_3(x, y)$, *see* equation (35).

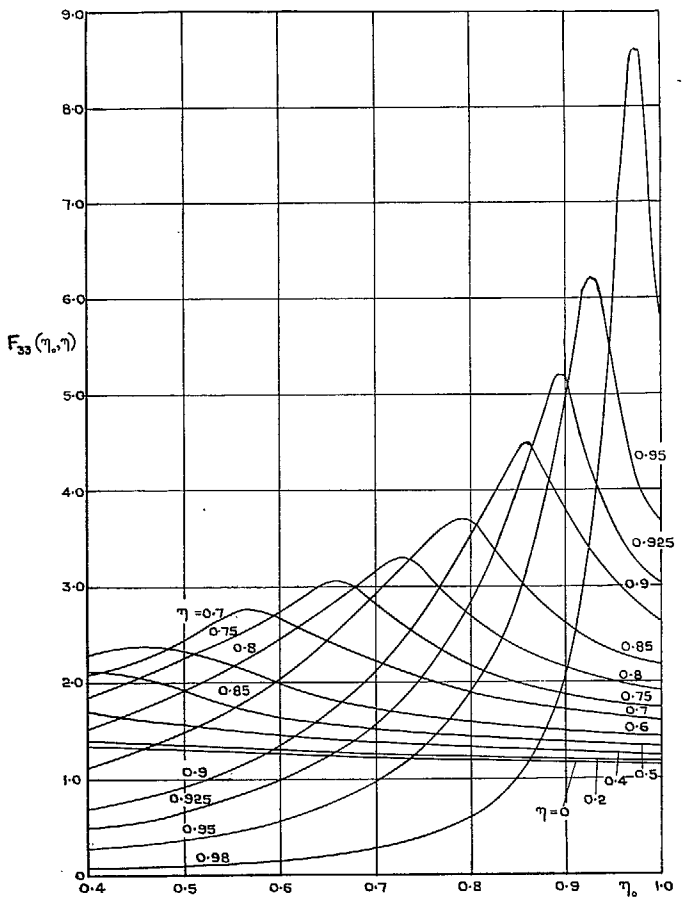

FIG. 8. Factor for $C(x)s(x)\ \{d\eta_0(x)/dx\}$ in $l_3(x, y)$, *see* equation (35).

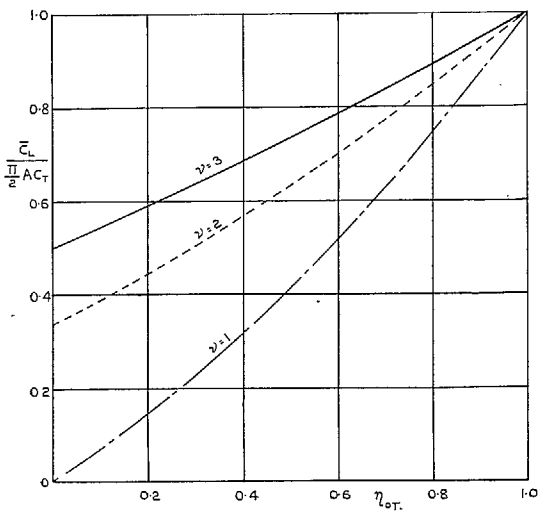

FIG. 9. Lift coefficients for various spanwise downwash distributions at the trailing edge, *see* Fig. 1.

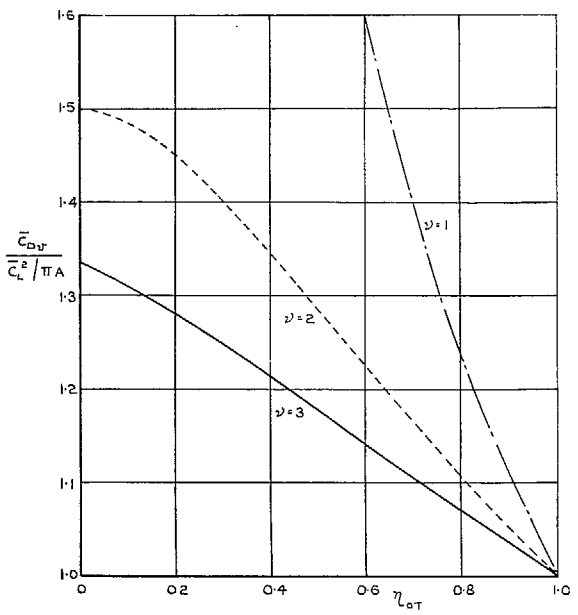

FIG. 10. Vortex-drag factors for various spanwise downwash distributions at the trailing edge, *see* Fig. 1.

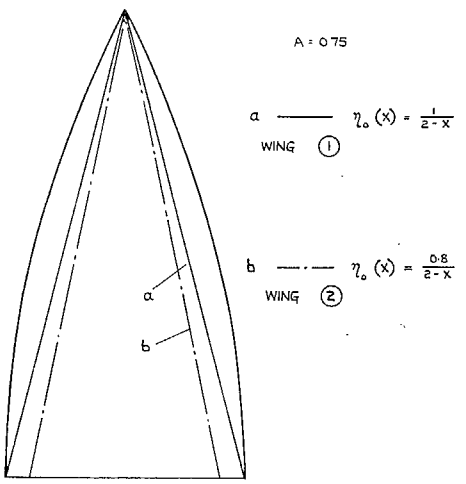

FIG. 11. Planform and shoulder positions for the calculated examples.

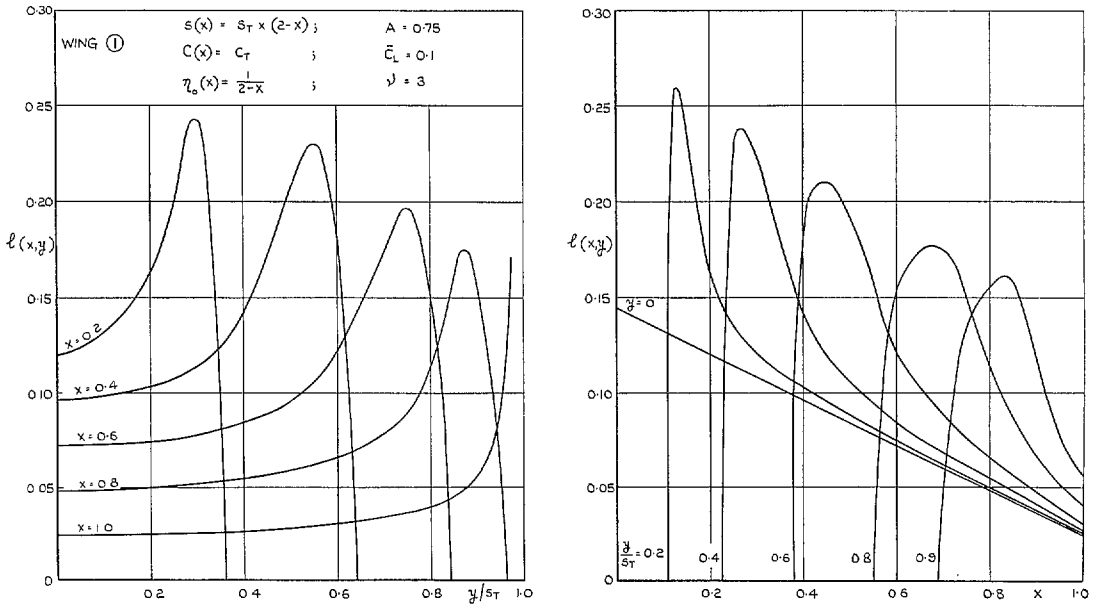

FIG. 12. Local load distributions.

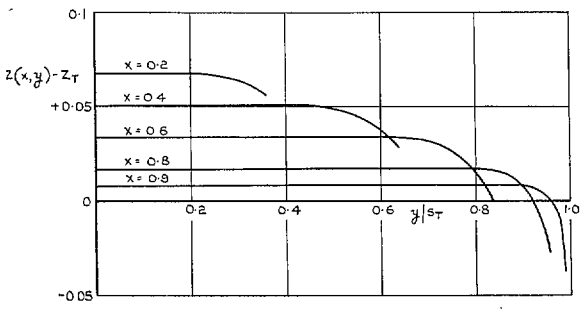

FIG. 13. Spanwise section shapes.

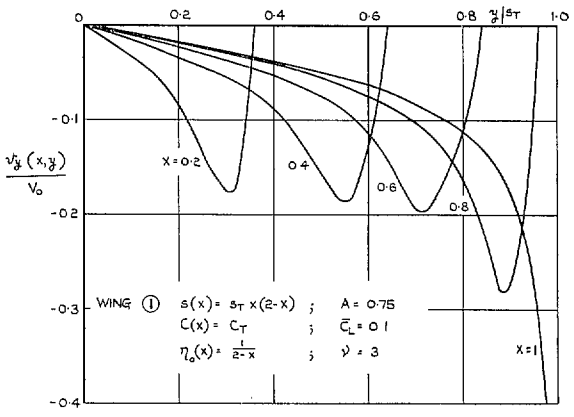

FIG. 14. Spanwise velocity component on upper surface.

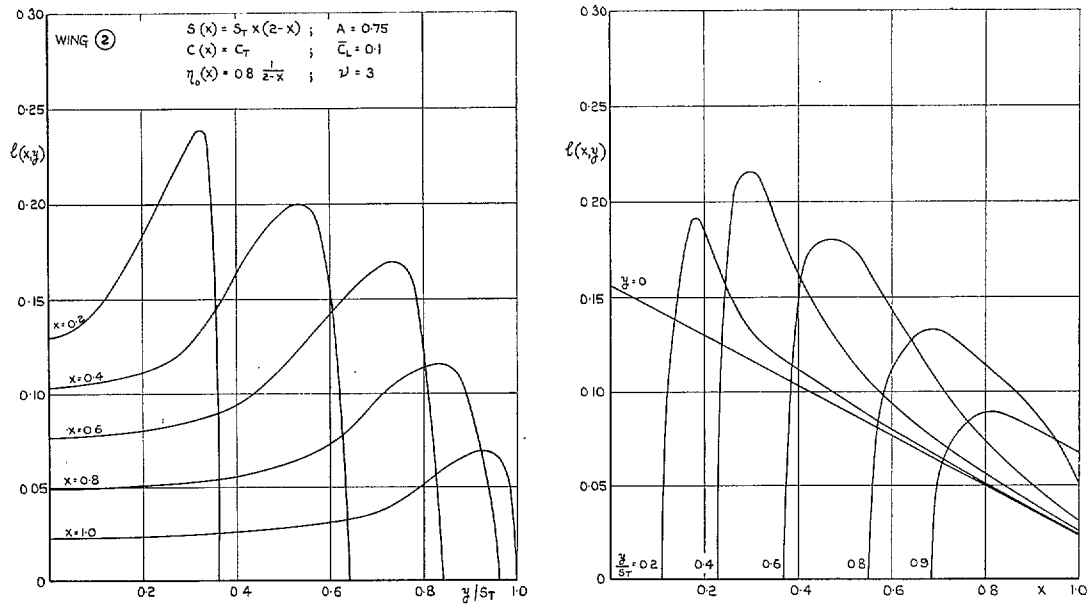

FIG. 15. Local load distributions.

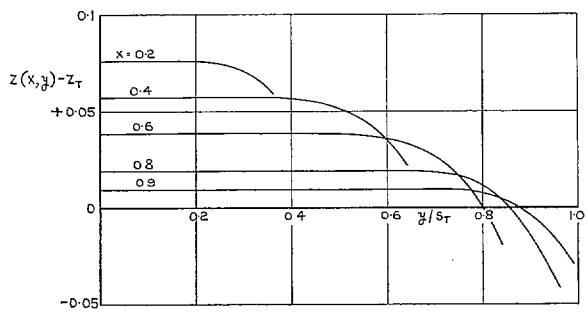

FIG. 16. Spanwise section shapes.

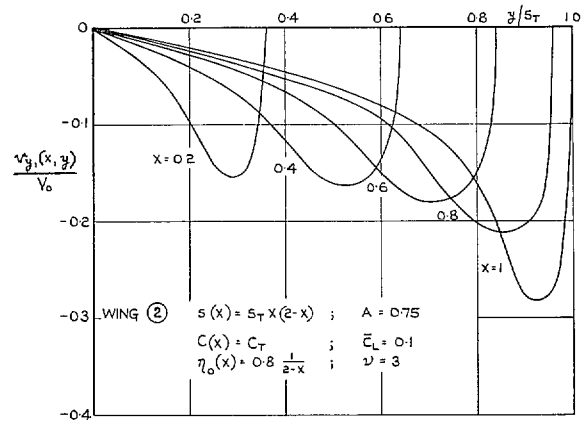

FIG. 17. Spanwise velocity component on upper surface.

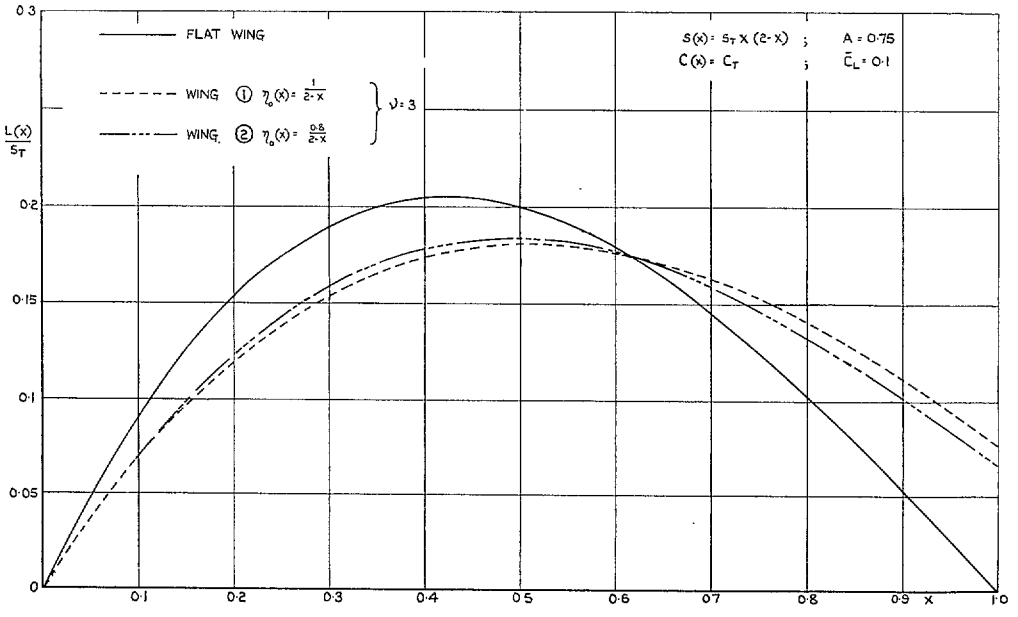

FIG. 18. Chordwise distributions of the cross load.

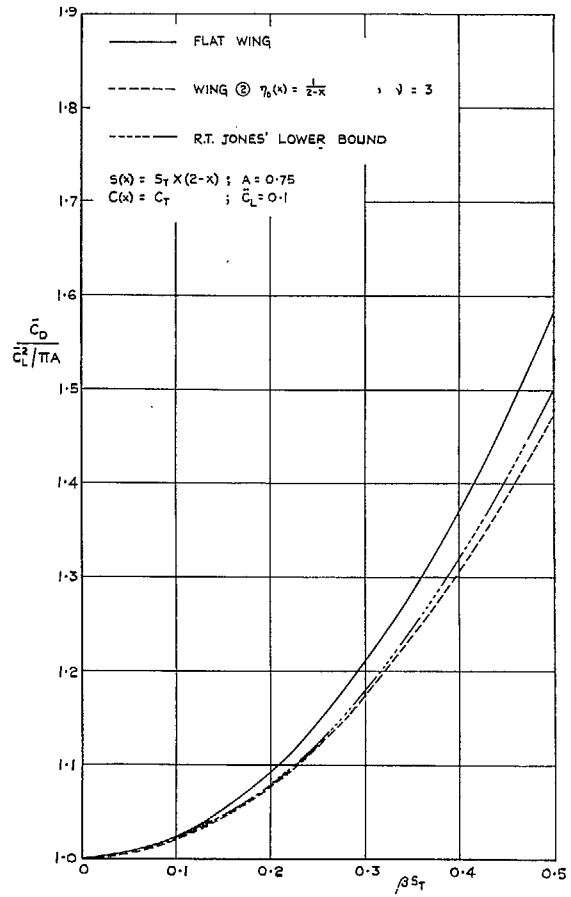

FIG. 19. Lift-dependent drag factors.

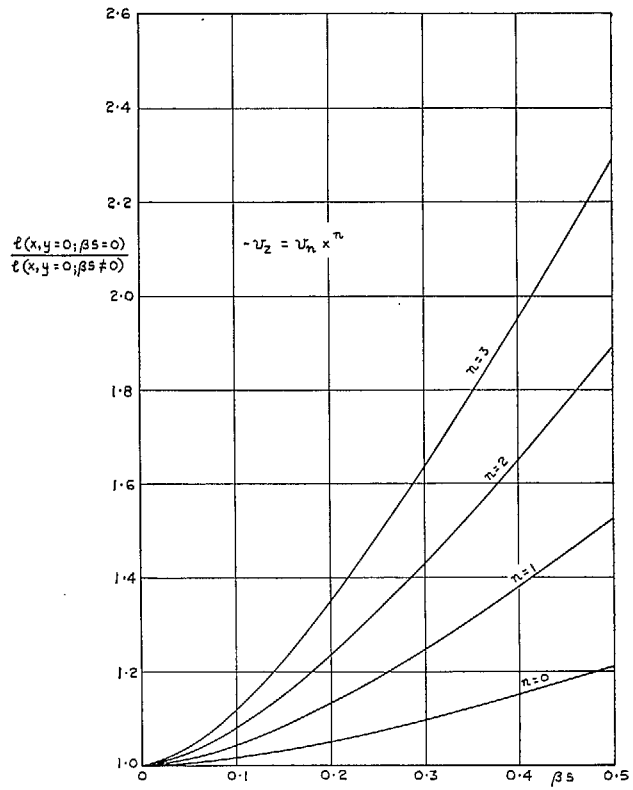

FIG. 20. Comparison of the loads at the centre section of warped delta wings calculated by linear theory (from Ref. 15) and by slender-wing theory.

(91392) Wt. 66/2301 K.5 6/65 Hw.

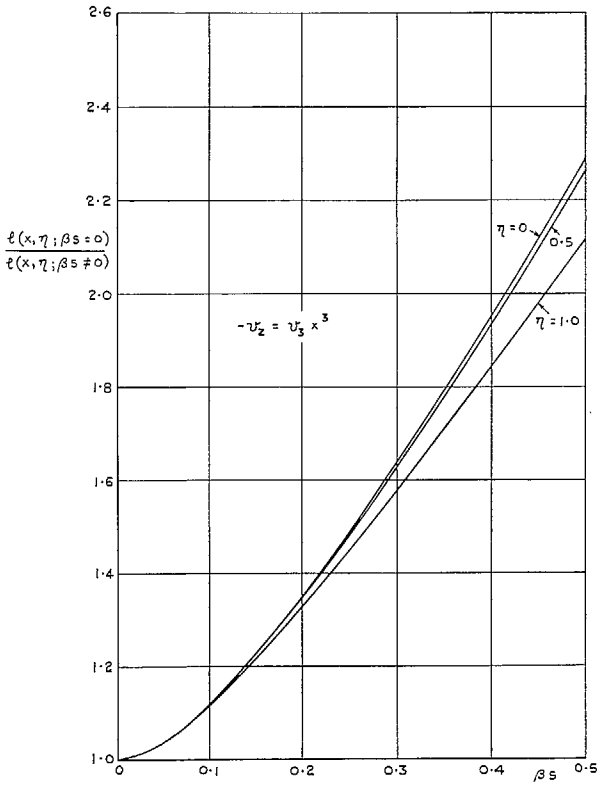

FIG. 21. Comparison of local loads on a warped delta wing calculated by linear theory (from Ref. 15) and by slender-wing theory.

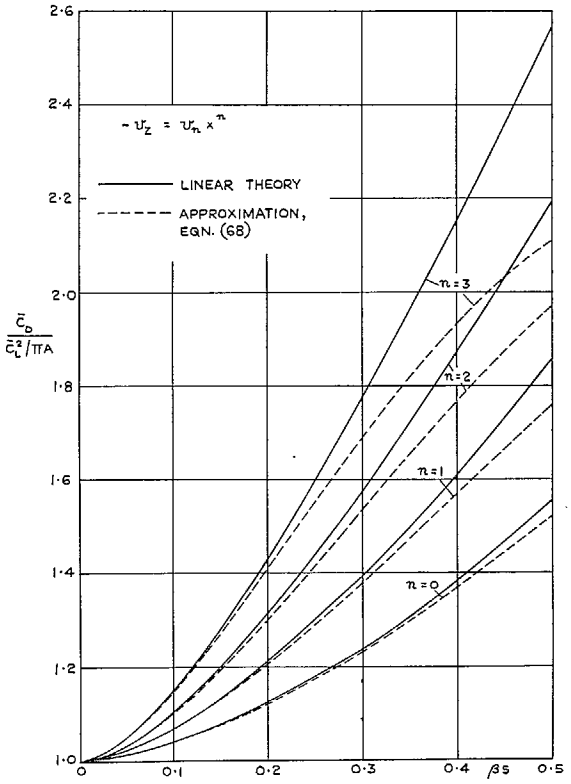

FIG. 22. Comparison of lift-dependent drag factors for warped delta wings calculated by linear theory and by an approximate method.

Publications of the Aeronautical Research Council

ANNUAL TECHNICAL REPORTS OF THE AERONAUTICAL RESEARCH COUNCIL (BOUND VOLUMES)

1945 Vol. I. Aero and Hydrodynamics, Aerofoils. £6 10*s*. (£6 13*s*. 6*d*.)
Vol. II. Aircraft, Airscrews, Controls. £6 10*s*. (£6 13*s*. 6*d*.)
Vol. III. Flutter and Vibration, Instruments, Miscellaneous, Parachutes, Plates and Panels, Propulsion. £6 10*s*. (£6 13*s*. 6*d*.)
Vol. IV. Stability, Structures, Wind Tunnels, Wind Tunnel Technique. £6 10*s*. (£6 13*s*. 3*d*.)

1946 Vol. I. Accidents, Aerodynamics, Aerofoils and Hydrofoils. £8 8*s*. (£8 11*s*. 9*d*.)
Vol. II. Airscrews, Cabin Cooling, Chemical Hazards, Controls, Flames, Flutter, Helicopters, Instruments and Instrumentation, Interference, Jets, Miscellaneous, Parachutes. £8 8*s*. (£8 11*s*. 3*d*.)
Vol. III. Performance, Propulsion, Seaplanes, Stability, Structures, Wind Tunnels. £8 8*s*. (£8 11*s*. 6*d*.)

1947 Vol. I. Aerodynamics, Aerofoils, Aircraft. £8 8*s*. (£8 11*s*. 9*d*.)
Vol. II. Airscrews and Rotors, Controls, Flutter, Materials, Miscellaneous, Parachutes, Propulsion, Seaplanes, Stability, Structures, Take-off and Landing. £8 8*s*. (£8 11*s*. 9*d*.)

1948 Vol. I. Aerodynamics, Aerofoils, Aircraft, Airscrews, Controls, Flutter and Vibration, Helicopters, Instruments, Propulsion, Seaplane, Stability, Structures, Wind Tunnels. £6 10*s*. (£6 13*s*. 3*d*.)
Vol. II. Aerodynamics, Aerofoils, Aircraft, Airscrews, Controls, Flutter and Vibration, Helicopters, Instruments, Propulsion, Seaplane, Stability, Structures, Wind Tunnels. £5 10*s*. (£5 13*s*. 3*d*.)

1949 Vol. I. Aerodynamics, Aerofoils. £5 10*s*. (£5 13*s*. 3*d*.)
Vol. II. Aircraft, Controls, Flutter and Vibration, Helicopters, Instruments, Materials, Seaplanes, Structures, Wind Tunnels. £5 10*s*. (£5 13*s*.)

1950 Vol. I. Aerodynamics, Aerofoils, Aircraft. £5 12*s*. 6*d*. (£5 16*s*.)
Vol. II. Apparatus, Flutter and Vibration, Meteorology, Panels, Performance, Rotorcraft, Seaplanes. £4 (£4 3*s*.)
Vol. III. Stability and Control, Structures, Thermodynamics, Visual Aids, Wind Tunnels. £4 (£4 2*s*. 9*d*.)

1951 Vol. I. Aerodynamics, Aerofoils. £6 10*s*. (£6 13*s*. 3*d*.)
Vol. II. Compressors and Turbines, Flutter, Instruments, Mathematics, Ropes, Rotorcraft, Stability and Control, Structures, Wind Tunnels. £5 10*s*. (£5 13*s*. 3*d*.)

1952 Vol. I. Aerodynamics, Aerofoils. £8 8*s*. (£8 11*s*. 3*d*.)
Vol. II. Aircraft, Bodies, Compressors, Controls, Equipment, Flutter and Oscillation, Rotorcraft, Seaplanes, Structures. £5 10*s*. (£5 13*s*.)

1953 Vol. I. Aerodynamics, Aerofoils and Wings, Aircraft, Compressors and Turbines, Controls. £6 (£6 3*s*. 3*d*.)
Vol. II. Flutter and Oscillation, Gusts, Helicopters, Performance, Seaplanes, Stability, Structures, Thermodynamics, Turbulence. £5 5*s*. (£5 8*s*. 3*d*.)

1954 Aero and Hydrodynamics, Aerofoils, Arrester gear, Compressors and Turbines, Flutter, Materials, Performance, Rotorcraft, Stability and Control, Structures. £7 7*s*. (£7 10*s*. 6*d*.)

Special Volumes

Vol. I. Aero and Hydrodynamics, Aerofoils, Controls, Flutter, Kites, Parachutes, Performance, Propulsion, Stability. £6 6*s*. (£6 9*s*.)
Vol. II. Aero and Hydrodynamics, Aerofoils, Airscrews, Controls, Flutter, Materials, Miscellaneous, Parachutes, Propulsion, Stability, Structures. £7 7*s*. (£7 10*s*.)
Vol. III. Aero and Hydrodynamics, Aerofoils, Airscrews, Controls, Flutter, Kites, Miscellaneous, Parachutes, Propulsion, Seaplanes, Stability, Structures, Test Equipment. £9 9*s*. (£9 12*s*. 9*d*.)

Reviews of the Aeronautical Research Council

1949–54 5*s*. (5*s*. 5*d*.)

Index to all Reports and Memoranda published in the Annual Technical Reports

1909–1947 R. & M. 2600 (out of print)

Indexes to the Reports and Memoranda of the Aeronautical Research Council

Between Nos. 2451–2549: R. & M. No. 2550 2*s*. 6*d*. (2*s*. 9*d*.); Between Nos. 2651–2749: R. & M. No. 2750 2*s*. 6*d*. (2*s*. 9*d*.); Between Nos. 2751–2849: R. & M. No. 2850 2*s*. 6*d*. (2*s*. 9*d*.); Between Nos. 2851–2949: R. & M. No. 2950 3*s*. (3*s*. 3*d*.); Between Nos. 2951–3049: R. & M. No. 3050 3*s*. 6*d*. (3*s*. 9*d*.); Between Nos. 3051–3149: R. & M. No. 3150 3*s*. 6*d*. (3*s*. 9*d*.); Between Nos. 3151–3249: R. & M. No. 3250 3*s*. 6*d*. (3*s*. 9*d*.); Between Nos. 3251–3349: R. & M. No. 3350 3*s*. 6*d*. (3*s*. 10*d*.)

Prices in brackets include postage

Government publications can be purchased over the counter or by post from the Government Bookshops in London, Edinburgh, Cardiff, Belfast, Manchester, Birmingham and Bristol, or through any bookseller

Printed and published by
HER MAJESTY'S STATIONERY OFFICE

To be purchased from
York House, Kingsway, London w.c.2
423 Oxford Street, London w.1
13A Castle Street, Edinburgh 2
109 St. Mary Street, Cardiff
39 King Street, Manchester 2
50 Fairfax Street, Bristol 1
35 Smallbrook, Ringway, Birmingham 5
80 Chichester Street, Belfast 1
or through any bookseller

Printed in England

S.O. Code No. 23-3406